Enhanced upward motion through the troposphere over the tropical western Pacific and its implications for the transport of trace gases from the troposphere to the stratosphere

Kai Qie [1], Wuke Wang[2], Wenshou Tian [1*], Rui Huang[1], Mian Xu[1], Tao Wang[1], Yifeng Peng[1]

[1]*College of Atmospheric Sciences, Lanzhou University, Lanzhou 730000, China*

[2] *Department of Atmospheric Science, China University of Geosciences, Wuhan 430074, China*

*Corresponding author: Wenshou Tian (wstian@lzu.edu.cn)

Abstract

The tropical western Pacific (TWP) is a preferential area of air uplifting from the surface to the upper troposphere. A significantly intensified upward motion through the troposphere over the TWP in the boreal wintertime (November to March of the next year, NDJFM) has been detected using multiple reanalysis datasets. The upward motion over the TWP is intensified at rates of 8.0±3.1% decade^{-1} and 3.6±3.3% decade^{-1} in NDJFM at 150 hPa from 1958 to 2017 using JRA55 and ERA5 reanalysis datasets, while the MERRA2 reanalysis data show a 7.5±7.1% decade^{-1} intensified upward motion for the period 1980-2017. Model simulations using the Whole Atmosphere Community Climate Model, version 4 (WACCM4) suggest that warming global sea surface temperatures (SSTs), particularly SSTs over the eastern maritime continent and tropical western Pacific, play a dominant role in the intensification of the upward motion by strengthening the Pacific Walker circulation and enhancing the deep convection over the TWP. Using CO as a tropospheric tracer, the WACCM4 simulations show that an increase of CO at a rate of 0.4 ppbv decade^{-1} at the layer 150-70 hPa in the tropics is mainly resulted from the global SST warming and the subsequent enhanced upward motion over the TWP in the troposphere and strengthened tropical upwelling of Brewer-Dobson (BD) circulation in the lower stratosphere. This implies that more tropospheric trace gases and aerosols from both natural maritime source and outflow from polluted air from South Asia may enter the stratosphere through the TWP region and affect the stratospheric chemistry and climate.

Keywords: Upward motion; Troposphere-to-stratosphere transport; Tropical western Pacific; Trend; Sea surface temperature

1 Introduction

The tropical western Pacific (TWP) is a critical region for tropical and global climate (e.g., Webster et al., 1996; Hu et al., 2020). It has the largest area of warm sea surface temperature (exceeding 28 ^{o}C) which fuels intense and massive deep convection and thus is the largest source of latent heat and water vapor into the atmosphere (Webster and Lukas, 1992). The TWP region is also the most important source of tropospheric air entering the stratosphere due to the strong upward motion and deep convection over this region (e.g., Fueglistaler et al., 2004; Pan et al., 2016). Through the TWP region, tropospheric trace gases, e.g., the natural maritime bromine-containing substances and outflow from anthropogenic emissions from South Asia, are lifted to the upper troposphere and lower stratosphere (UTLS) by the strong upward motion and the deep convection and subsequently into the stratosphere by the large-scale upwelling (e.g., Levine et al., 2007, 2008; Navarro et al., 2015), which affect the ozone concentration and other chemical processes in the stratosphere (e.g., Feng et al., 2007; Sinnhuber et al., 2009). At the same time, the TWP region has the lowest cold-point tropopause temperature (CPTT) over the globe and plays an important role in controlling the water vapor concentration in the stratosphere (e.g., Fueglistaler et al., 2009; Newell and Gould-Steward, 1981; Pan et al., 2016; Randel and Jensen, 2013). The TWP is an important region for tropospheric trace gases being transported from the troposphere to the stratosphere, and therefore influencing the stratospheric chemistry (e.g., Fueglistaler et al., 2004; Levine et al., 2007; Krüger et

al., 2008; Pan et al., 2016).

The TWP was thought to be the main pathway of the troposphere-to-stratosphere transport. A concept of "stratospheric fountain" was proposed by Newell and Gould-Steward (1981), which suggested that the poor-water vapor air in the stratosphere stems mainly from the TWP region. However, following studies using the observational and reanalysis data showed that there is subsidence at the near-tropopause level over the maritime continent, which is named as the "stratospheric drain" (Gettelman et al., 2000; Sherwood, 2000; Fueglistaler et al., 2004). Further studies verified that the large-scale transport from the tropical tropopause layer (TTL) to the stratosphere is dominated by the upward branch of the Brewer-Dobson (BD) circulation (Brewer, 1949; Dobson, 1956; Holton et al., 1995) while the local upwelling may play a minor role (e.g., Levine et al., 2007; Fueglistaler et al., 2009; Schoeberl et al., 2018).

Though the vertical transport from TTL to the lower stratosphere is dominated by the BD circulation, numerous studies confirmed that the TWP region is an important pathway of the surface air entering the TTL (Fueglistaler et al., 2004; Levine et al., 2007; Krüger et al., 2008; Haines and Esler, 2014). Based on a trajectory model, Fueglistaler et al. (2004) pointed out that approximately 80% of the trajectories ascending into the stratosphere from the TTL are originated from the TWP region. Bergman et al. (2012) suggested that the tropospheric air over the TWP enters the stratosphere mainly in boreal winter, while less air over the TWP could be transported into the stratosphere during boreal summer. Other studies also found that the TWP

region is an important source of the tropospheric trace gases in the TTL (e.g., Newton et al., 2018; Pan et al., 2016; Wales et al., 2018), even the polluted air from East Asia could be transported rapidly to Southeast Asia by meridional winds and subsequently be elevated to the tropical upper troposphere by the strong upward motion and the deep convection (Ashfold et al., 2015). Hence, the strength of the upward motion over the TWP region during boreal winter is a key feature for understanding the variations of trace gases in the TTL and therefore important for stratospheric chemistry and climate.

The strength of the TWP upward motion is closely related to atmospheric circulation and deep convection. The ascending branch of the Pacific Walker circulation and the strong deep convection over the TWP allow rapid transport from the surface to the upper troposphere (Hosking et al., 2012). In association with global warming, atmospheric circulation, deep convection as well as the boundary conditions (e.g., sea surface temperature; SST) have been changed. For example, the Hadley cell has been extended to the subtropics and the Walker circulation over the Pacific has been shifted westward over the past decades (e.g., Lu et al., 2007; Garfinkel et al., 2015; Ma and Zhou, 2016). At the same time, SSTs over most of areas are getting warmer (Cane et al., 1997; Deser et al., 2010), which modulates the deep convection and atmospheric wave activities in the troposphere and then lead to changes of atmospheric circulations from the troposphere and the stratosphere (e.g., Garfinkel et al., 2013; Xie et al., 2012, 2014a; Wang et al., 2015; Hu et al., 2016; Lu et al., 2020). However, how the strength of the upward motion in the lower TTL over the TWP

region has been changed over the past decades remains unclear. In this study, we investigate the long-term trend of the upward motion over the TWP using JRA55, ERA5, and MERRA2 reanalysis datasets and different WACCM4 simulations as described in Section 2. The implication of the changes in the upward motion over the TWP to the transport of trace gases from the surface to the UTLS will be discussed in Section 3.

2 Data and method

Reanalysis data. To investigate the long-term trend of the upward motion over the TWP through the troposphere, three most recent reanalysis datasets, including JRA55 from the Japan Meteorological Agency (JMA), ERA5 from the European Centre for Medium Range Weather Forecasting (ECMWF) and MERRA2 from the National Aeronautics and Space Administration/Global Modeling and Assimilation Office (NASA/GMAO) are used in this study. The JRA55 is produced by a four dimensional variational (4D-Var) data assimilation system and provide 6-hourly data (Harada et al. 2016). It has a vertical resolution of 60 levels from the surface to 0.1 hPa and a high horizontal resolution (T319). It covers the period from 1958 to present, are interpolated to the standard pressure levels and 1.25°×1.25° horizontal mesh. More details could be found in Kobayashi et al., 2015. The ERA5 reanalysis is the newest generation product from the ECMWF (Hersbach et al., 2020). The ERA5 data are based on the Integrated Forecasting System (IFS) Cy41r2, which includes the improved model physics, core dynamics and data assimilation. The ERA5 has hourly output, a horizontal resolution of 31 km, and a vertical resolution of 137 levels

127 extending into the middle atmosphere (0.01 hPa) and covers the period from 1979 to
128 present. The ERA5 data also extend back to 1958, which is coinciding with the time
129 that radiosonde observations in the Arctic became more systematic and regular. It
130 should be noted that the ERA5 data suffer from a bias during 2000-2006, and are
131 replaced by the ERA5.1 data in this period here. The MERRA2 data are also used,
132 which are only accessible after 1980 (Gelaro et al., 2017). The MERRA2 data are
133 produced by NASA/GMAO using Goddard Earth Observing System model (GEOS),
134 which have 3-hourly temporal resolution, 72 vertical levels up to 0.01 hPa, and a
135 horizontal resolution of 0.5°×0.625°. Although the horizontal and vertical resolution
136 of MERRA2 data are similar to MERRA data, the MERRA2 data represent UTLS
137 processes better (Gelaro et al., 2017). The monthly mean air temperature, horizontal
138 wind fields and vertical velocity at different pressure levels are extracted from the
139 three Reanalysis datasets. In the present study, we mainly focus on the upward motion
140 over TWP region in NDJFM, which is defined as 20°S-10°N, 100°E-180° due to the
141 strong upward motion (Fig. 1) and significantly increasing trends of the upward
142 motion (Fig. 2) over there.

143 A special caution is needed because of the limitations of reanalysis data. The
144 reanalysis datasets assimilate observational data based on the ground- and
145 space-based remote sensing platforms to provide more realistic data products.
146 However, previous studies suggested that there are still uncertainties in the reanalysis
147 data (e.g., Simmons et al., 2014; Long et al., 2017; Uma et al., 2021). The accuracy of
148 the vertical velocity in reanalysis data sets has been evaluated by the Reanalysis

Intercomparison Project (Fujiwara et al., 2017), which is initiated by the Stratosphere-troposphere Processes And their Role in Climate (SPARC). Results of a comparison between the radar observed data and the reanalysis data indicate that the updrafts in the UTLS are captured well near the TWP even though there are still large biases in the reanalysis datasets and the updrafts from the JRA55 data are stronger than those from the ERA5 and MERRA2 data (Uma et al. 2021). Additionally, discontinuities in the reanalysis data due to different observing systems (for example, transition from TOVS to ATOVS) may still exist (e.g., Long et al., 2017), which could lead to uncertainties in the long-term trend of a certain meteorological field. Hitchcock (2019) suggested that the reanalysis uncertainty is larger in the radiosonde era (after 1958) than in the satellite era (after 1979), but the radiosonde era is of equivalent value to the satellite era because the dynamical uncertainty dominates in the both eras. The data in the radiosonde era (1958-1978) used in the present study may induce uncertainties in our results. Therefore, we discuss the trends for both the periods of 1958-2017 and 1980-2017. In addition, we combine three most recent reanalysis datasets (JRA55, ERA5, and MERRA2) to obtain relatively robust results.

Observed CO data. CO is used as a tropospheric tracer in this study to indicate the vertical transport from the near-surface to the upper troposphere and the lower stratosphere. The CO data used in the present study are from space-borne Microwave Limb Sounder (MLS; Livesey et al., 2015) observation and Measurements Of Pollution In The Troposphere instrument (MOPITT; Deeter et al., 2019). MLS is carried by Aura, which has a sun-synchronous orbit at 705 km with a 16-day repeat

cycle. MLS observations are made from 82°S to 82°N and cover the period from 2005 to the present. MLS provides the CO data from the upper troposphere to the mesosphere. MLS CO v4 level1 data used in the present study are processed using the recommended procedures (Livesey et al., 2015) and interpolated into a 5°×5° horizontal mesh. MOPITT CO data are also used for comparison. MOPITT instrument is aboard on the Terra satellite permitting retrievals of CO vertical profiles using both thermal-infrared and near-infrared measurements and has a field of view of 22 km×22 km. The Terra satellite was launched in 1999 with a 705 km sun-synchronous orbit. MOPITT provides the CO data from the surface to the upper troposphere during the period of 2000/03 to the present. Here, we use the daytime only MOPITT v8 level3 CO data. For comparison, we focus on the CO concentrations in MLS and MOPITT data at similar level (215 hPa in MLS data and 200 hPa in MOPITT data, respectively).

SST and outgoing longwave radiation (OLR) data. SST data are used in this study to investigate the relationship between the upward motion and SSTs. The SST data are from the HadISST dataset (1°×1° horizontal mesh) during 1958-2018 (Rayner et al., 2003). OLR is often utilized to reflect the deep convection in the tropics. The OLR data are extracted from NOAA Interpolated OLR dataset on a 2.5°×2.5° horizontal mesh during 1974/11-2018/03 (Liebmann and Smith, 1996).

Model simulations. A series of model simulations with the Whole Atmosphere Community Climate Model version 4 (WACCM4) are performed to find out the main impact factors of the trend of the upward motion over the TWP. The WACCM4 is a

chemical-climate model with a horizontal resolution of 1.9°×2.5° (Marsh et al., 2013). The WACCM4 has vertical 66 levels from the surface to 145 km with vertical resolution of approximately 1 km in the UTLS, which is numerously used to investigate the transport of the trace gases from the troposphere to the stratosphere (e.g., Randel et al., 2010; Xie et al., 2014b; Minganti et al., 2020). A hindcast simulation (Control simulation) is performed with observed greenhouse gases, solar irradiances, and prescribed SSTs (HadISST dataset is used) during 1955-2018. A single-factor controlling simulation (Fixsst simulation) is done for the same period with the same forcings, except that the global SSTs are fixed to the climatological mean values during 1955-2018 (long-term mean for each calendar month during 1955-2018).

To figure out the impact of the warming SST over the TWP region on the intensification of the upward motion over the TWP region, a couple of time-slice simulations (R1 and R2) are also integrated for 33 years. The SSTs over the eastern maritime continent and tropical western Pacific (20°S-20°N, 120°E-160°E) in the boreal wintertime (November to March of the next year, NDJFM) in R1 are prescribed as the climatological mean SSTs during 1998-2017, while the SSTs over other regions are fixed as the climatological mean SSTs during 1958-2017. The SSTs in R2 are the same as the SSTs in R1 except that the SSTs over the region (20°S-20°N, 120°E-160°E) in NDJFM are prescribed as the climatological mean SSTs during 1958-1977. Since the SSTs over the eastern maritime continent and tropical western Pacific (20°S-20°N, 120°E-160°E) show significantly warming trends, the SSTs

during 1998-2017 are higher than the SSTs during 1958-1977 (approximately 0.5 K). Hence, the difference between R1 and R2 reflects the impact of the warmed SSTs over the eastern maritime continent and tropical western Pacific (20°S-20°N, 120°E-160°E) on the atmospheric circulation. The first 3 years of the numeric simulations are not used in the present study to provide a spin-up.

Transformed Eulerian Mean (TEM) Calculation. To diagnose the changes in the BD circulation, the meridional and vertical velocities of the BD circulation are calculated by the TEM equations (Andrews and Mcintyre, 1976):

$$v^* = \bar{v} - \frac{1}{\rho}\left(\frac{\rho\overline{v'\theta'}}{\overline{\theta}_z}\right)_z$$

$$w^* = \bar{w} + \frac{1}{a\cos\varphi}\left(\cos\varphi\frac{\overline{v'\theta'}}{\overline{\theta}_z}\right)_\varphi$$

Where v^* and w^* denote the meridional and vertical velocities of the BD circulation; the overbar represents the zonal mean; the prime denotes the deviation from the zonal mean; θ, a, φ, and ρ indicate the potential temperature, the radius of the earth, the latitude, and the standard density.

Linear trends and the significance test. The linear trends are estimated using a simple least square regression method. The significances of the correlation coefficients, mean differences, and trends are determined via a two-tail Student's t-test. The confidence interval of trend is calculated using the following equation (Shirley et al., 2004): $\left(b - t_{1-\frac{\alpha}{2}}(n-2)\sigma_b, b + t_{1-\frac{\alpha}{2}}(n-2)\sigma\right)$

where b is the estimated slope, σ denotes the standard error of the slope, and

$t_{1-\frac{\alpha}{2}}(n-2)$ represents the value of t-distribution with the degree of freedom equal to n-2. α is the two-tailed confidence level. σ is calculated as: $\sigma = b\sqrt{\frac{\frac{1}{r^2}-1}{n-2}}$.

3 Results

3.1 Enhanced upward motion over the TWP

According to previous studies, the lapse-rate tropopause is a good proxy to separate the tropospheric and the stratospheric dynamic behavior (vertical motion dominated and horizontal mixing dominated, respectively) over the TWP (Pan et al., 2019). Since the lapse-rate tropopause over the TWP in the boreal winter is near 100 hPa (not shown), we utilize the vertical velocity at 150 hPa to reflect the vertical transport in the upper troposphere. Figure 1 shows mean values of the vertical velocity at 150 hPa for each month averaged over 60 years from 1958 to 2017. The TWP region at the UTLS level has strong upward motion due to the frequent intense deep convection and the Pacific Walker circulation. It is noteworthy that there is strong upward motion at 150 hPa in NDJFM over the TWP, while the upward motion in other months shifts northward corresponding to the Asia summer monsoon. This is consistent with previous studies (Newell and Gould-Steward, 1981; Bergman et al., 2012). Therefore, we mainly focus on the changes in the upward motion in NDJFM, which is more important to the transport of air over the TWP from the lower troposphere to the TTL compared to the summer months (as shown in Fig. 1) and subsequently to the lower stratosphere. As seen in Figs. 1a-c and 1k-l, the upward motion (w) at 150 hPa is most evident over the region 20°S-10°N, 100°E-180°, which

256 is used to indicate the TWP in the following analysis. The climatological mean 150
257 hPa vertical velocity (*w*) in NDJFM in ERA5 during 1958-2017 and MERRA2 during
258 1980-2017 are also given in Supplementary Fig. 1. Comparing with the 150 hPa *w* in
259 NDJFM using JRA5, the 150 hPa *w* in ERA5 and MERRA2 data shows larger values
260 (maximum larger than 1.5 m s^{-1}) over the land areas but smaller values (minimum less
261 than -0.4 m s^{-1}) over the marine area. Notably, the 150 hPa *w* shows no subsidence
262 over the maritime continent, while there is descending motion over the maritime
263 continent at 100 hPa (Supplementary Fig. 2), which is referred to the "stratospheric
264 drain" (Gettleman et al., 2000; Sherwood, 2000).

265 Figure 2 displays the linear trends of *w* in the upper (150 hPa), middle (500 hPa)
266 and lower (700 hPa) troposphere in NDJFM from 1958 to 2017 using JRA55, ERA5,
267 and MERRA2 reanalysis datasets. The 150 hPa *w* increased significantly over most
268 areas of the TWP during 1958-2017 (Fig. 2). At the same time, the upward motion
269 over the TWP in the lower and middle troposphere also mainly shows positive trends
270 (Figs. 2d and g). This indicates that the upward motion over the TWP is increasing
271 through the troposphere from 1958 to 2017. Such an enhancement of the upward
272 motion over the TWP is evident in all three reanalysis datasets used here (JRA55,
273 ERA5, and MERRA2), although there are also some differences between the three
274 reanalysis datasets. For example, the trends of the horizontal winds in the upper
275 troposphere in MERRA2 (Fig. 2c) are larger than those in JRA55 and ERA5 (Figs. 2a
276 and b). There are negative trends of vertical velocity in JRA55 and ERA5 while
277 positive trends of vertical velocity in MERRA2 over the northern Pacific. However,

these differences are mainly due to the different time periods which are used to calculate the linear trends in JRA55 (1958-2017), ERA5 (1958-2017) and MERRA2 (1980-2017). Supplementary Fig. 3 gives the trends of *w* and horizontal winds in NDJFM during 1980-2017 derived from JRA55, ERA5, and MERRA2 data, which shows insignificant differences between these reanalysis datasets. The trend patterns of the horizontal winds in JRA55, ERA5, and MERRA2 are consistent with each other (Supplementary Fig. 3). For the trends of vertical velocity, significant positive trends over the TWP region can be noted in the JRA55, ERA5, and MERRA2 datasets, although the trends in ERA5 are slightly weaker than those in JRA55 and MERRA2 (Fig. 2 and Supplementary Fig. 3). Comparing to the negative trends of the vertical velocity over the central Pacific in JRA55 and ERA5, the negative trends in MERRA2 extend more northward (Supplementary Fig. 3).

The time series of the upward motion intensity over the TWP from different datasets are given in Fig. 3. The intensity of the upward motion over the TWP used in Fig. 3 is simply defined as the area-averaged upward mass flux at a specific level, and the standardized intensity is calculated as the intensity divided by the standard deviation of the intensity at the corresponding level. The intensity of the upward motion over the TWP at 150 hPa increased significantly in NDJFM during last decades, which can be confirmed by all the three reanalysis datasets (Fig. 3). The intensity of the upward motion over the TWP at 150 hPa increased $3.0\pm1.2\times10^{8}$ kg s^{-1} $decade^{-1}$ ($8.0\pm3.1\%$ $decade^{-1}$), $1.3\pm1.2\times10^{8}$ kg s^{-1} $decade^{-1}$ ($3.6\pm3.3\%$ $decade^{-1}$), and $3.0\pm2.8\times10^{8}$ kg s^{-1} $decade^{-1}$ ($7.5\pm7.1\%$ $decade^{-1}$) in JRA55, ERA5, and MERRA2 data,

300 respectively. As shown in Figs. 3b and c, the intensity of the upward motion at 500
301 hPa and 700 hPa in JRA55 and the intensity of the upward motion at 500 hPa in
302 ERA5 over the TWP also increased significantly at 95% confidence level
303 ($4.6\pm2.6\times10^8$ kg s^{-1} $decade^{-1}$, $2.9\pm1.7\times10^8$ kg s^{-1} $decade^{-1}$, and $2.5\pm2.5\times10^8$ kg s^{-1}
304 $decade^{-1}$, respectively). The increasing trends of the intensity of the upward motion at
305 700 hPa in ERA5 and at 500 hPa and 700 hPa in MERRA2 are significant at the 90%
306 confidence level at rates of $1.9\pm1.6\times10^8$ kg s^{-1} $decade^{-1}$, $5.4\pm5.3\times10^8$ kg s^{-1} $decade^{-1}$
307 and $3.9\pm3.8\times10^8$ kg s^{-1} $decade^{-1}$, respectively. This suggests a comprehensive
308 enhancement of vertical velocity through the whole troposphere, which is evident
309 from the surface to 100 hPa (Supplementary Fig. 4). It can also be inferred that the
310 upward motions over the TWP increased at different rates during the past decades due
311 to the difference between JRA55, ERA5, and MERRA2 data. Hence, caution is
312 suggested when investigating the trend of the upward motion over the TWP using the
313 reanalysis data. While the trace gases in the TTL are modulated by the upward motion
314 and subsequent vertical transport (e.g., Garfinkal et al., 2013; Xie et al., 2014b), such
315 a strengthening of the upward motion over the TWP may lead to more tropospheric
316 trace gases in the TTL.

317 The changes in the atmospheric circulation at the UTLS level in the tropics are
318 closely related to the changes in the tropical deep convection and SSTs (e.g., Levine
319 et al., 2008; Garfinkal et al., 2013; Xie et al., 2020). Here, the trends of observed OLR
320 provided by NOAA (see Section 2) in NDJFM during 1974-2017 are shown in Fig. 4a.
321 Though the time period of the observed OLR data is shorter than the time period we

322 analyzed, the changes in OLR could partly reflect the changes in the deep convection
323 during 1958-2017. The OLR shows significantly negative trends over the TWP which
324 indicates intensified deep convection over the TWP. The OLR trend pattern is very
325 similar to the trend pattern of the 150 hPa *w* (Figs. 2a-c), which indicates that the
326 increasing trends of 150 hPa *w* are closely related to the intensified deep convection
327 over the TWP. The intensified deep convection not only lead to the strengthened
328 upward motion in the UTLS (Highwood and Hoskins, 1998; Ryu and Lee, 2010), but
329 also result in the decreased temperature near the tropopause which plays a dominant
330 role in modulating the lower stratospheric water vapor concentration (e.g., Hu et al.,
331 2016; Wang et al., 2016). Corresponding to the enhanced deep convection over the
332 TWP, the CPTT derived from JRA55 data (see Fig. 4b) shows significantly decreasing
333 trends over the TWP in NDJFM during 1958-2017, which is consistent with Xie et al.,
334 (2014a). However, negative trends are also found in other regions in low and
335 mid-latitudes, except over the central and east Pacific. It should be noted that the
336 CPTT from different reanalysis datasets may show different trends even for the
337 satellite period (Tegtmeier et al., 2020). Additionally, the JRA55 data before 1978
338 may also lead to uncertainties in the CPTT trends. Caution is needed when discussing
339 the trends of CPTT from reanalysis datasets.

340 The changes in the deep convection over the tropical Pacific may be related to
341 the changes in the Pacific Walker circulation. The Pacific Walker circulation shows a
342 significant intensification over the past decades (e.g., Meng et al., 2012; L'Heureux et
343 al., 2013; McGregor et al., 2014). The vertical velocity at 500 hPa and 150 hPa shows

significantly positive trends over the TWP in NDJFM during 1958-2017 (Fig. 2). Meanwhile, the lower tropospheric zonal wind shows easterly trends over the tropical Pacific, while the upper tropospheric zonal wind shows westerly trends over the tropical Pacific, which suggests a strengthened Pacific Walker circulation and is consistent with previous studies (Hu et al., 2016; Ma and Zhou, 2016).

The strengthened Pacific Walker circulation is closely related to the changes in the SSTs (e.g., Meng et al., 2012; Ma and Zhou, 2016). The trends of the SSTs in NDJFM during 1958-2017 are shown in Fig. 4c. The SST shows significantly warming trends almost over the world except the central Pacific in NDJFM during 1958-2017. In addition, the intensity of the upward motion over the TWP is significantly correlated with the SST (Fig. 4d), which suggests that the SST has important effects on the upward motion over the TWP. The correlation coefficient in Fig. 4d shows a La Niña-like pattern and indicates that the ENSO events exert important impacts on the upward motion over the TWP (Levine et al., 2008). The SSTs over the TWP are mainly positively correlated with the upward motion intensity over the TWP with negative correlations shown over the western maritime continent, while the SSTs over tropical central, eastern Pacific, and Indian Ocean show negative correlations with the intensity of the upward motion over the TWP. The SSTs over the Atlantic Ocean are poorly correlated with the upward motion intensity over the TWP (not shown). This result suggests that the changes in global SSTs may be the primary driver of the strengthened Pacific Walker circulation, which leads to enhanced deep convection and intensified upward motion over the TWP.

It could be found that there are extreme minima (1982, 1991, and 1997) in Fig. 3, which may be related to the El Niño events occurred in these years. To further figure out the impact of ENSO events on the upward motion over the TWP, Supplementary Fig. 5 displays the time series of the standardized intensity of the upward motion over the TWP at 150 hPa, 500 hPa, and 700 hPa in NDJFM in JRA55, ERA5, and MERRA2 with the ENSO signal removed using the linear regression method (Hu et al., 2018; Qie et al., 2021). The extreme minima (1982, 1991, and 1997) become much weaker in Supplementary Fig. 5 than those in Fig. 3, which indicates that the El Niño events are responsible for the extreme minima. The upward motions over the TWP at 150 hPa, 500 hPa, and 700 hPa in NDJFM in JRA55, ERA5, and MERRA2 still show statistically significant increasing trends after removing the ENSO signal in Supplementary Fig. 5, which suggests that ENSO events exert limited impacts on the trends of the upward motion over the TWP in NDJFM during 1958-2017.

3.2 Simulated trend of the upward motion over the TWP and its potential mechanism

To verify the impact of SST on the trend of the upward motion over the TWP, a couple of model simulations with WACCM4 are employed in the following analysis. Consistent with the results shown using the reanalysis data (Figs. 2a-c), the simulated 150 hPa *w* (Control simulation) shows significantly increasing trends over the TWP and decreasing trends over the tropical eastern Pacific in NDJFM during 1958-2017 (Fig. 5a). Additionally, the 150 hPa *w* simulated in the Fixsst simulation shows weak trends over the TWP (Fig. 5b). The difference between the Control and the Fixsst

388 simulations suggests that the trends of the 150 hPa *w* over the TWP region is
389 dominated by the changes in the global SSTs during 1958-2017. There are also
390 significantly positive trends of the vertical velocity over the TWP in the lower (700
391 hPa) and middle troposphere (500 hPa) in the Control simulation, while the zonal
392 winds are also enhanced over the tropical Pacific. The vertical velocity over the TWP
393 in the Fixsst simulation shows weak negative trends and the changes in zonal winds
394 over the tropical Pacific are very weak. This confirms the dominant role of the
395 changes in global SSTs on the enhancement of the Walker circulation.

396 Previous studies found that the changes in the intensity of the Pacific Walker
397 circulation and the stratospheric residual circulation are closely related to the changes
398 in tropical SST (Meng et al., 2012; Tokinaga et al., 2012; Lin et al., 2015). As
399 suggested by the correlation coefficients between the upward motion at 150 hPa over
400 the TWP and SSTs in Fig. 4d, warmer SSTs over the tropical central and eastern
401 Pacific, and Indian Ocean may lead to a weakened upward motion over the TWP
402 (negative correlation). The warming trends of SSTs over the eastern maritime
403 continent and tropical western Pacific may result in an intensification of the upward
404 motion over the TWP. To verify the impact of the changes in the SSTs over eastern
405 maritime continent and tropical western Pacific on the trends of the upward motion
406 over the TWP, a couple of single-factor controlling time-slice simulations (R1 and R2)
407 are performed with only SSTs over eastern maritime continent and tropical western
408 Pacific (20°S-20°N, 120°E-160°E) in NDJFM changed in these two simulations. In
409 R1, the SSTs over the eastern maritime continent and tropical western Pacific are

410 prescribed as the climatological mean SSTs during 1958-2017, while the SSTs over
411 the eastern maritime continent and tropical western Pacific in R2 are prescribed as the
412 climatological mean SSTs during 1958-1977 (more details are given in the section 2).
413 The differences of the wind fields between R1 and R2 are shown in Fig. 6. The 150
414 hPa *w* shows significantly positive anomalies over the TWP and negative anomalies
415 over the tropical eastern Pacific, which is consistent with the trends of the 150 hPa *w*
416 in the Control simulation and the reanalysis datasets (Figs. 2 and 5). The upward mass
417 flux over the TWP at 150 hPa increased approximately 27% in the R1 comparing with
418 R2 due to the warming SSTs over the eastern maritime continent and tropical western
419 Pacific (approximately 0.5 K). The upward motion in the lower and middle
420 troposphere over the TWP shows increasing trends due to the enhanced convergence
421 induced by the warmer SSTs over the TWP. This result is consistent with Hu et al.
422 (2016), which suggested that the increased zonal gradient of the SSTs over the
423 tropical Pacific could lead to a strengthened Pacific Walker circulation and an
424 enhanced upward motion over the TWP. Therefore, the warmer SSTs over the TWP
425 could contribute largely to the trend of the upward motion over the TWP in NDJFM
426 during 1958-2017.

427 The changes in the OLR simulated in WACCM4 associated with the changes in
428 the global SSTs are shown in Fig. 7. There are significantly enhanced deep convection
429 as indicated by OLR over the TWP due to the strengthened convergence in the
430 Control simulation, while the deep convection shows weak and even decreasing
431 trends over the TWP in the Fixsst simulation (Figs. 7a and b). The enhanced deep

convection over the TWP could lead to the enhancing trends of the upward motion. Hence, it can be inferred that the changes in the global SSTs are responsible for the intensification of the Pacific Walker circulation, and the enhanced deep convection and a stronger upward motion over the TWP which could extend to the upper troposphere.

3.3 Implications for the concentrations of water vapor and CO in the TTL and lower stratosphere.

Previous studies showed that the enhanced deep convection and upward motion could lead to increased CO in the UTLS (e.g., Duncan et al., 2007; Livesey et al., 2013). At the same time, water vapor mixing ratios in the UTLS may increase due to the enhanced upward motion which could bring more wet air from low altitude to high altitude (e.g., Rosenlof, 2003; Lu et al., 2020). However, the water vapor mixing ratios in the lower stratosphere also depend on the tropopause temperature (e.g., Highwood and Hoskins, 1998; Garfinkel et al., 2018; Pan et al., 2019). Hence, the relationship between the intensity of upward motion and the water vapor concentration in the UTLS is complex. Here, the relationship between the trends of the upward motion over the TWP and the changes in CO and water vapor in the ULTS simulated with WACCM4 are analyzed.

The trends of CPTT, the 100 hPa streamfunction, and the water vapor concentration are shown based on the Control and the Fixsst simulation as well as their difference in Figs. 7d-i. The changes in the deep convection could lead to the changes in the atmospheric circulation by releasing the latent heat. The changes in the

tropical deep convection lead to a Rossby-Kelvin wave response at the UTLS level and then induce the changes in the air temperature near the tropopause (e.g., Gill, 1980; Highwood and Hoskins, 1998). The trends of the 100 hPa streamfunction show a Rossby wave response over the TWP and a Kelvin wave response over the tropical eastern Pacific in the Control simulation (Fig. 7d), which is caused by the changes in the deep convection over the tropical Pacific. The Rossby-Kelvin wave response further leads to the decrease the CPTT over the TWP and the increase of the CPTT over the tropical eastern Pacific. Previous studies suggest that the lower stratospheric water vapor is mainly influenced by the coldest temperature near the tropopause (e.g., Garfinkel et al., 2018; Zhou et al., 2021). Since the TWP has the coldest CPTT in the boreal winter (e.g., Pan et al., 2016), the significantly decreased CPTT over the TWP may result in significantly dried lower stratosphere (Fig. 7g). The intensity of the upward motion over the TWP shows negative correlations with the concentration of the tropical lower stratospheric water vapor (not shown). Hence, the enhanced upward motion over the TWP may correspond to a dried lower stratosphere. The CPTT shows weak trends over the TWP, and the tropical water vapor shows insignificant trends at 70 hPa in the Fixsst simulation. The comparison between the Control simulation and the Fixsst simulation suggests that the trends of the deep convection, the CPTT, and the lower stratospheric water vapor concentration in the tropics in NDJFM during 1958-2017 are dominated by the trends of the global SSTs, while other external forcings may play minor roles.

Generally, the intensified upward motion may lead to more tropospheric trace

gases lifting to the upper troposphere and entering the lower stratosphere (e.g., Rosenlof, 2003; Lu et al., 2020). Here we use CO as a tropospheric tracer to detect the possible influences of the enhanced upward motion over the TWP on the transportation of the tropospheric trace gases to the upper troposphere and the lower stratosphere. Due to the data limitation, it is not possible to show the corresponding changes of trace gases by observations in NDJFM during 1958-2017. Here, the trends of CO at around 200 hPa from MOPITT and MLS observations are shown in the Fig. 8. The CO increased significantly over the TWP in NDJFM in the upper troposphere from the MOPITT (at 200 hPa during 2000-2017) and MLS data (at 215 hPa during 2005-2017). The concentration of MLS CO over the TWP is approximately 80 ppbv at 215 hPa from MLS observations and 70 ppbv at 200 hPa from MOPITT observations, which is consistent with previous study (e.g., Huang et al., 2016). The MLS CO data show that the area-averaged CO increased approximately 2.0±3.7 ppbv decade^{-1} over the TWP in NDJFM during 2005-2017. The area-averaged MOPITT CO data show a stronger increase of approximately 5.0±3.1 ppbv decade^{-1} at 200 hPa from 2000 to 2017 (significant at the 95% confidence level). It should be pointed out that the linear trends of CO are calculated based on the satellite data which only cover 14 or 18 years due to the data limitation. Hence, the linear trends of CO may have uncertainties particularly in the regions with large interannual variations. To partially overcome this shortage, the trends of MLS CO at 215 hPa during time periods of 2005-2016, 2006-2016, 2006-2017, and 2007-2016 and the trends of MOPITT CO at 200 hPa during time periods of 2000-2016, 2001-2016, 2001-2017, and 2002-2016

are shown in Supplementary Fig. 6. It could be found that the CO in the upper troposphere increased robustly over the TWP from both the MLS and MOPITT data. Overall, though the observed CO only covers less than 20 years, the results from the satellite data suggest a possible impact of the intensified upward motion over the TWP on the trace gases in the upper troposphere.

To further illustrate the impacts of the enhanced upward motion on the trace gas in the upper troposphere and lower stratosphere, the Control and Fixsst simulations with WACCM4 are used. The trends of the CO concentrations from the Control and Fixsst simulations as well as their differences are shown in Fig. 9. The tropical CO at 150 hPa shows significantly increasing trends both in the Control and the Fixsst simulations at rates of 3.4 ppbv decade^{-1} and 3.2 ppbv decade^{-1}, respectively, (Figs. 9a and b). This suggests that the surface emission of the CO exerts the most important effect on the increase of the tropical CO concentration. The differences of the CO trends at 150 hPa between the Control simulation and the Fixsst simulation are also displayed in Fig. 9c. Since the surface emission inventories of the two simulations are the same, it can be inferred that the trends of the CO concentration in Fig. 9c are mainly caused by the changes in the atmospheric circulation induced by the changes in the global SSTs. The difference of the CO concentration at 150 hPa between the Control simulation and the Fixsst simulation shows a significantly increasing trend at a rate of 0.2±0.1 ppbv decade^{-1} over the TWP (significant at the 95% confidence level). At the same time, decreasing trends over the central Africa exist, which resembles to the trend patterns of the vertical velocity in the lower TTL and the deep

convection (Figs. 5i and 7c). This indicates that the enhanced deep convection in the TWP lead to the strengthened upward motion over the TWP, which results in an extra 6% increasing trend of CO in the upper troposphere over the TWP. It could also be found that CO also increased in the mid latitudes of the southern hemisphere (Fig. 9c). According to previous studies, the CO perturbation from the Indonesian fires at upper troposphere could be transported to the tropical Indian Ocean by easterly winds and then to the subtropics in the southern hemisphere through the southward flow during boreal winter. The CO perturbation then spreads rapidly circling the globe following the subtropical jet (Duncan et al., 2007). This is consistent with our results which show intensified northerlies over the subtropical Indian Ocean (15°S-25°S, 60°E-100°E) at a rate of approximately 0.2 m s^{-1} $decade^{-1}$ and strengthened westerlies over the subtropical Indian Ocean and western Pacific (20°N-35°N, 60°E-160°E) at a rate of approximately 0.3 m s^{-1} $decade^{-1}$ (Figs. 5c and f).

The trends of the zonal mean CO concentration from model simulations are displayed in Figs. 10a-c. The zonal mean CO shows significantly increasing trends at all levels in the Control simulation and the Fixsst simulation, while the difference of the zonal mean CO between the Control simulation and the Fixsst simulation shows significantly increasing trends in the TTL but negative trends in the middle troposphere in the tropics and the Northern Hemisphere. At the same time, the difference of CO concentration between the Control simulation and the Fixsst simulation averaged in the western Pacific (100°E-180°E) shows significantly increasing trends in the tropics (20°S-10°N) from the surface to the TTL (Fig. 10f).

The CO in the layer 150-70 hPa over the TWP increased 3.2 ppbv decade^{-1} and 2.8 ppbv decade^{-1} in the Control and Fixsst simulations in NDJFM during 1958-2017, respectively. And the CO difference between the Control and Fixsst simulations increased 0.4±0.2 ppbv decade^{-1} (significant at the 95% confidence level) in the layer 150-70 hPa over the TWP, which suggests that the intensifying upward motion over the TWP and the tropical upwelling of BDC could lead to an extra 14% increasing trend of CO. This indicates that the increased zonal mean CO in the TTL (Fig. 10c) is mainly transported through the western Pacific bands and highlights the importance of the upward motion over the TWP in elevating trace gases from the surface to the upper troposphere.

To understand the CO trends in the Control and Fixsst simulations and their differences, the trends of vertical velocity averaged over the globe and the TWP band are given in Fig. 11. The zonal mean *w* shows weak and even decreasing trends in the tropics while the *w* over the TWP intensified in the Control simulation in NDJFM during 1958-2017. This is consistent with Fig. 5. While the SSTs fixed to climatological values, the zonal mean *w* shows weak trends and the *w* over the TWP shows significantly negative trends. The changes in the global SSTs therefore leads to the increase of the *w* over the TWP region as indicated in the differences between the two simulations in Fig. 11f. In summary, the CO shows increasing trends (3.5 ppbv decade^{-1}) at 150 hPa over the TWP in NDJFM during 1958-2017 induced by the changes in the surface emissions and the upward motion. The trends of CO at 150 hPa over the TWP in NDJFM during 1958-2017 in the Fixsst simulation mainly include

564 the impact induced by the increased surface emissions since the upward motion over
565 the TWP in the Fixsst simulation shows weak trends. The difference between the
566 Control and Fixsst simulations indicates that the enhanced tropospheric upward
567 motion over the TWP forced by the changes in the global SSTs leads to some extra
568 increase of CO concentrations in the upper troposphere. It should be mentioned that
569 the increasing trends of CO in the lower troposphere in Fig. 10f may be mainly caused
570 by the changes in the horizontal winds. Girach and Nair (2014) suggested that
571 enhanced deep convection and the subsequent intensified upward motion may lead to
572 a decreased CO concentration in the lower troposphere and an increased CO
573 concentration in the upper troposphere. The trends of horizontal winds at 925 hPa are
574 shown in Supplementary Fig. 8c. There are northerly trends over east Asia and
575 northeasterly trends near the south Asia (Supplementary Fig. 8c), which suggests that
576 more CO-rich air from east Asia and south Asia could be transported to the TWP in
577 the Control simulation comparing to the Fixsst simulation. Since the CO
578 concentration in the lower troposphere over the northern Pacific is higher than that
579 over southern Pacific, the northerly trends over the western and central Pacific may
580 also contribute to the increased CO in the lower troposphere over the TWP in Fig. 10f.
581 As discussed in the Introduction, the tropospheric trace gases enter the
582 stratosphere mainly through the large-scale tropical upwelling associated with the BD
583 circulation. The trends of the BD circulation in different model simulations as well as
584 their differences are displayed in Fig. 12. The tropical upwelling of BDC (w^*)
585 calculated using the TEM formula increased significantly in the lower stratosphere

586 over past decades as seen in the JRA55 data and the Control simulation (Figs. 12a and
587 12b). We found that the 70 hPa upward mass flux in NDJFM in the tropics
588 (15°S-15°N) increased 2.8±1.9% decade^{-1} (significant at the 95% confidence level) in
589 the JRA55 data from 1958 to 2017 (Fig. 12a) and 4.6±4.3% decade^{-1} (significant at
590 the 95% confidence level) in the MERRA2 data from 1980 to 2017 (Supplementary
591 Fig. 7b). From the ERA5 data, the 70 hPa upward mass flux in NDJFM increased in
592 the north hemisphere (0-15°N) at a rate of 5.0±2.8% decade^{-1} (significant at the 95%
593 confidence level), but decreased significantly in the south hemisphere (0-15°S) during
594 1958-2017 (Supplementary Fig. 7a). On average, the trend of the 70 hPa upward mass
595 flux in NDJFM in the tropics (15°S-15°N) is not significant in ERA5. In fact, many
596 previous studies have investigated the trends of BDC. For example, Abalos et al.
597 (2015) investigated the trends of BDC derived from JRA55, MERRA, and
598 ERA-Interim data during 1979-2012 and suggested that the BDC in JRA55 and
599 MERRA significantly strengthened throughout the layer 100-10 hPa with a rate of
600 2-5% decade^{-1}, while the BDC in ERA-Interim shows weakening trends. Diallo et al.
601 (2021) compared the trends of the BDC in the ERA5 and ERA-Interim during
602 1979-2018 and pointed out that the BDC in the ERA-Interim shows weakening trend
603 and the BDC in the ERA5 strengthened at a rate of 1.5% decade^{-1} which is more
604 consistent with other studies. In the present study, we only focus on the trend of the
605 BDC in the wintertime (NDJFM) in the tropics (15°S-15°N) during 1958-2017, which
606 may lead to some differences between our result and that in the previous studies.
607 Overall, the trends of the tropical upwelling of BDC derived from JRA55, MERRA2

608 data and the Control simulation are similar to that in previous studies using both
609 reanalysis datasets and model results (e.g., Butchart et al., 2010; Abalos et al., 2015;
610 Fu et al., 2019; Rao et al., 2019; Diallo et al., 2021). However, the tropical upwelling
611 of the BDC decreased in ERA5 data in the tropics (15°S-15°N), which are different
612 from the results in JRA55 and MERRA2.

613 In the Fixsst simulation, the trend of w^* is much weaker and not significant in
614 most areas. The changes in the global SSTs therefore play an important role in the
615 intensification of the shallow branch of the BDC as shown by the differences between
616 the two simulations in Fig. 12d. In summary, the tropical upwelling of the BDC is
617 likely strengthened as shown in JRA55 and MERRA2 reanalyses as well as model
618 simulations, although there are some uncertainties since the ERA5 data show a
619 negative trend. This may impact on the transport of the tropospheric trace gases from
620 the TTL to a higher altitude. The increased concentration of CO in the UTLS in Fig.
621 9c and 10f may be due to a combined effect of the strengthened tropical upwelling of
622 the BD circulation and the enhanced upward motion over the TWP. The enhancement
623 of upward motion over the TWP, which transported more tropospheric trace gases to
624 the upper troposphere, works together with the strengthened BD circulation under
625 global warming may lead to an increase of tropospheric trace gases over the TWP in
626 the lower stratosphere.

627 **4 Summary and Discussion**

628 The recent trends of the upward motion from the lower to the upper troposphere
629 in boreal winter over the TWP is investigated for the first time based on the JRA55,

ERA5, MERRA2 datasets and four WACCM4 simulations (more details could be found in Section 2). The upward motion at 150 hPa over the TWP in NDJFM increased 8±3.1% decade^{-1} and 3.6±3.3% decade^{-1} in NDJFM from 1958 to 2017 in JRA55 and ERA5 reanalysis datasets, respectively. Despite the possible discontinuities between the radiosonde era (after 1958) and the satellite era (after 1979), the upward motion at 150 hPa over the TWP in NDJFM increased 7.5±7.1% decade^{-1} during 1980-2017 in MERRA2 data. Such intensification of the upward motion over the TWP also exist in the middle- and lower-troposphere in NDJFM in JRA55, ERA5, and MERRA2, which can be confirmed by the WACCM4 model simulations. Comparing the results between the Control and Fixsst simulations with WACCM4, it is found that the trend of the upward motion over the TWP is closely related to the changes in global SSTs, especially the SST warming over the eastern maritime continent and tropical western Pacific (see the results from the experiments R1 and R2 in Fig. 7). Warmer SSTs over the eastern maritime continent and tropical western Pacific (approximately 0.5 K) lead to a strengthened Pacific Walker circulation, enhanced deep convection and approximately 27% intensified upward motion at 150 hPa over the TWP as shown by the results from the experiments R1 and R2. The enhanced deep convection over the TWP could lead to a dryer lower stratosphere over the TWP, as the strong upward motion and the Rossby-Kelvin wave responses induce a colder tropopause over the TWP. It should be pointed out that the results in the present study are mainly based on the reanalyses data, and some uncertainties may exist. More observational data are expected to be used to obtain a

652 more robust result in the future.

653 Results from the Control simulation indicate that the CO concentrations
654 increased significantly from the surface to the stratosphere over the TWP. The CO at
655 150 hPa increased at a rate of approximately 3.4 ppbv decade^{-1} with increased surface
656 emissions and the enhanced upward motion over the TWP. Specifically, an
657 enhancement of tropospheric upward motion and subsequent upward transport of
658 trace gases over the TWP lead to an extra 6% increasing trend of CO concentrations
659 in the upper troposphere.

660 Furthermore, the upward mass fluxes at 70 hPa in the tropics (15°S-15°N) show
661 strengthening trends at rates of 2.8±1.9% decade^{-1} and 4.6±4.3% decade^{-1} in JRA55
662 data (during 1958-2017) and MERRA2 data (during 1980-2017) in NDJFM,
663 respectively, which is consistent with previous studies (e.g., Butchart et al., 2010; Fu
664 et al., 2019; Rao et al., 2019). However, such enhancement in tropical upward mass
665 flux at 70 hPa has large uncertainties since the ERA5 data show a negative and
666 insignificant trend (Supplementary Fig. 7a). The results from the Control and Fixsst
667 simulations indicate that the elevated CO in the upper troposphere is further uplifted
668 to the lower stratosphere by the intensified tropical upwelling of the BD circulation
669 due mainly to global SST warming and lead to an increase of CO in the lower
670 stratosphere. An extra 14% increasing trend of CO at the layer 150-70 hPa over the
671 TWP is derived from the Control and Fixsst simulations.

672 Tropospheric trace gases and aerosols have important impacts on the
673 stratospheric processes if they enter the stratosphere. For example, ozone-depleting

substances, CH_4 and N_2O could influence on the stratospheric ozone significantly (e.g., Shindell et al., 2013; Wang et al., 2014; WMO, 2018), which also modify the temperature in the stratosphere significantly through their strong radiative effects. Water vapor in the lower stratosphere, in particular, has a significant warming effect on the surface climate (Solomon et al., 2010). Therefore, changes of trace gases in the UTLS have important impacts on both tropospheric and stratospheric climate. Our results suggest that the upward motion over the TWP and the vertical component of the BDC at the lower stratosphere level have been intensified. These results suggest that the emission from the maritime continent and surrounding areas may play a more important role in the stratospheric processes and the global climate. In addition, more very short lived substances emitted from the tropical ocean could be elevated to the TTL by the enhanced convection and then transported into the stratosphere by the large-scale uplifts and exert important effects on the stratospheric chemistry. However, the quantitative impacts of the intensified upward motion over the TWP on tropospheric and stratospheric trace gases and aerosols and their climate feedbacks await further investigation using more observations and model simulations.

Competing interests. The authors declare that they have no conflict of interest.

Author contributions. WT designed the study. WW provided suggestions about the statistical methods and model simulations. KQ ran the models and wrote the first draft. RH, MX, and TW contributed to the manuscript writing. YP provided the data used in

the study. All authors contributed to the improvement of the results.

Acknowledgements. This research is supported by Strategic Priority Research Program of Chinese Academy of Sciences (XDA17010106), the National Natural Science Foundation of China (42075055) and the Supercomputing Center of Lanzhou University.

The authors gratefully acknowledge the data used in the present study provided by the corresponding scientific groups. The JRA55 data are from:
http://rda.ucar.edu/datasets/ds628.0/.
The SST data is obtained from HadISST:
https://www.metoffice.gov.uk/hadobs/hadisst/data/download.html.
The ERA5 data and ERA5.1 data are extracted from:
https://cds.climate.copernicus.eu/#!/search?text=ERA5&type=dataset.
The MERRA2 data are downloaded from:
https://search.earthdata.nasa.gov/search?q=MERRA2&fst0=Atmosphere.
The OLR data are from https://psl.noaa.gov/data/gridded/data.interp_OLR.html.

References:

Abalos, M., Legras, B., Ploeger, F., and Randel, W. J.: Evaluating the advective Brewer-Dobson circulation in three reanalyses for the period 1979-2012, J. Geophys. Res., 120,7534-7554, doi:10.1002/2015JD023182, 2015.

Andrews, D. G., and Mcintyre, M. E.: Planetary waves in horizontal and vertical shear: the generalized eliassen-palm relation and the mean zonal acceleration, J. Atmos. Sci., 33, 2031–2048, 1976

Ashfold, M. J., Pyle, J. A., Robinson, A. D., Meneguz, E., Nadzir, M. S. M., Phang, S. M., Samah, A. A., Ong, S., Ung, H. E., Peng, L. K., Yong, S. E., and Harris, N. R.

723 P.: Rapid transport of East Asian pollution to the deep tropics, Atmos. Chem.
724 Phys., 15, 3565-3573, doi:10.5194/acp-15-3565-2015, 2015.
725 Bergman, J. W., Jensen, E. J., Pfister, L., and Yang, Q.: Seasonal differences of
726 vertical-transport efficiency in the tropical tropopause layer: On the interplay
727 between tropical deep convection, large-scale vertical ascent, and horizontal
728 circulations, J. Geophys. Res., 117, D05302, doi:10.1029/2011JD016992, 2012.
729 Brewer, A. M.: Evidence for a world circulation provides by the measurements of
730 helium and water vapor distribution in the stratosphere, Q. J. R. Meteorol. Soc.,
731 75, 351–363, 1949.
732 Butchart, N., Cionni, I., Eyring, V., Shepherd, T. G., Waugh, D. W., Akiyoshi, H.,
733 Austin, J., Brühl, C., Chipperfield, M. P., Cordero, E., Dameris, M., Deckert, R.,
734 Dhomse, S., Frith, S. M., Garcia, R. R., Gettelman, A., Giorgetta, M. A.,
735 Kinnison, D. E., Li, F., Mancini, E., McLandress, C., Pawson, S., Pitari, G.,
736 Plummer, D. A., Rozanov, E., Sassi, F., Scinocca, J. F., Shibata, K., Steil, B., and
737 Tian, W.: Chemistry–Climate Model simulations of twenty-first century
738 stratospheric climate and circulation changes, J. Climate, 23, 5349–5374,
739 https://doi.org/10.1175/2010JCLI3404.1, 2010.
740 Cane, M. A., Clement, A. C., Kaplan, A., Kushnir, Y., Pozdnyakov, D., and Seager, R.,
741 et al.: Twentieth-century sea surface temperature trends, Science, 275(5302),
742 957-960, DOI: 10.1126/science.275.5302.957, 1997.
743 Deeter, M. N., Edwards, D. P., Francis, G. L., Gille, J. C., Mao, D., Martinez-Alonso,
744 S., Worden, H. M., Ziskin, D., and Andreae, M. O.: Radiance-based retrieval bias
745 mitigation for the MOPITT instrument: the version 8 product, Atmos. Meas.
746 Tech., 12, 4561–4580, https://doi.org/10.5194/amt-12-4561-2019, 2019.
747 Deser, C., Phillips, A. S., and Alexander, M. A.: Twentieth century tropical sea surface
748 temperature trends revisited, Geophys. Res. Lett., 37(10), L10701,
749 doi:10.1029/2010GL043321, 2010.
750 Diallo, M., Ern, M., and Ploeger, F.: The advective Brewer‐Dobson circulation in
751 the ERA5 reanalysis: climatology, variability, and trends, Atmos. Chem. Phys.,

21, 7515 – 7544, https://doi.org/10.5194/acp-21-7515-2021, 2021.

Dobson G. M. B.: Origin and distribution of the polyatomic molecules in the atmosphere, Proc. R. Soc. Lond. Ser. A. 236: 187-193, 1956.

Duncan, B. N., Logan J. A., Bey, I., Megretskaia, I. A., Yantosca, R. M., Novelli, P. C., Jones, N. B. and Rinsland, C. P.: Global budget of CO, 1988-1997: Source estimates and validation with a global model, J. Geophys. Res., 112, D22301, doi:10.1029/2007JD008459, 2007.

Feng, W., Chipperfifield, M. P., Dorf, M., Pfeilsticker, K., and Ricaud, P.: Mid-latitude ozone changes: studies with a 3-D CTM forced by ERA-40 analyses, Atmos. Chem. Phys., 7, 2357 – 2369, doi:10.5194/acp-7-2357-2007, 2007.

Fu, Q., Solomon, S., Pahlavan, H. A., and Lin, P.: Observed changes in Brewer–Dobson circulation for 1980–2018, Environ. Res. Lett., 14, 114 026, https://doi.org/10.1088/1748-9326/ab4de7, 2019.

Fueglistaler, S., Desller, A. E., Dunkerton, T. J., Folkins, I., Fu, Q., and Mote P.: Tropical tropopause layer, Rev. Geophys., 47(1), RG1004, doi:10.1029/2008RG000267, 2009.

Fueglistaler, S., Wernli, H., and Peter, T.: Tropical troposphere-to-stratosphere transport inferred from trajectory calculations, J. Geophys. Res., 109, D03108, doi:10.1029/2003JD004069, 2004.

Fujiwara, M., Wright, J. S., Manney, G. L., Gray, L. J., Anstey, J., Birner, T., Davis, S., Gerber, E. P., Harvey, V. L., Hegglin, M. I., Homeyer, C. R., Knox, J. A., Krüger, K., Lambert, A., Long, C. S., Martineau, P., Molod, A., Monge-Sanz, B. M., Santee, M. L., Tegtmeier, S., Chabrillat, S., Tan, D. G. H., Jackson, D. R., Polavarapu, S., Compo, G. P., Dragani, R., Ebisuzaki, W., Harada, Y., Kobayashi, C., McCarty, W., Onogi, K., Pawson, S., Simmons, A., Wargan, K., Whitaker, J. S., and Zou, C.-Z.: Introduction to the SPARC Reanalysis Intercomparison Project (S-RIP) and overview of the reanalysis systems, Atmos. Chem. Phys., 17, 1417-1452, https://doi.org/10.5194/acp-17-1417-2017, 2017

Garfinkel, C. I., Waugh, D. W., and Polvani, L. M.: Recent Hadley cell expansion: The role of internal atmospheric variability in reconciling modeled and observed

782 trends, Geophys. Res. Lett., 42(24), 10824-10831,
783 https://doi.org/10.1002/2015GL066942, 2015
784 Garfinkel, C. I., Waugh, D. W., Oman, L. D., Wang, L., and Hurwitz, M. M.:
785 Temperature trends in the tropical upper troposphere and lower stratosphere:
786 Connections with sea surface temperatures and implications for water vapor and
787 ozone, J. Geophys. Res., 118, 9658-9672, doi:10.1002/jgrd.50772, 2013.
788 Garfinkel, C. O., Gordon, A., Oman, L. D., Li, F., Davis, S., and Pawson, S.:
789 Nonlinear response of tropical lower-stratospheric temperature and water vapor
790 to ENSO, Atmos. Chem. Phys., 18, 4597-4615,
791 https://doi.org/10.5194/acp-18-4597-2018, 2018.
792 Gelaro, R., Mccarty, W., and Suárez, M. J.: The modern-era retrospective analysis for
793 research and applications, version 2 (merra-2), J. Climate, 30(14), 5419-5454,
794 https://doi.org/10.1175/JCLI-D-16-0758.1, 2017
795 Gettelman, A., Holton, J. R., and Douglass, A. R.: Simulations of water vapor in the
796 lower stratosphere and upper troposphere, J. Geophys. Res., 105(D7), 9003-9023,
797 https://doi.org/10.1029/1999JD901133, 2000.
798 Gill, A. E.: Some simple solutions for heat-induced tropical circulation, Q. J. R.
799 Meteorolog. Soc., 106, 447-462, doi:10.1002/qj.49710644905, 1980.
800 Girach, I. A., and Nair, P. R.: Carbon monoxide over Indian region as observed by
801 MOPITT, Atmos. Environ., 99, 599-609,
802 http://dx.doi.org/10.1016/j.atmosenv.2014.10.019, 2014.
803 Haines, P. E., and Esler, J. G.: Determination of the source regions for surface to
804 stratosphere transport: An Eulerian backtracking approach, Geophys. Res. Lett.,
805 41, 1343-1349, doi:10.1002/2013GL058757, 2014.
806 Harada, Y., Kamahori, H., Kobayashi, C., Endo, H., Kobayashi, S., Ota, Y., Onoda, H.,
807 Onogi, K., Miyaoka, K., and Takahashi, K.: The JRA-55 Reanalysis:
808 Representation of atmospheric circulation and climate variability, J. Meteorol.
809 Soc. Jpn., 94(3), 269-302, https://doi.org/10.2151/jmsj.2016-015, 2016.
810 Hersbach, H., Bell, B., Berrisford, P., Hirahara, S., Horányi, A., Muñoz-Sabater, J.,
811 and Nicolas, J., et al.: The ERA5 global reanalysis, Q. J. R. Meteorol. Soc., 146,

812 1999-2049, DOI: 10.1002/qj.3803, 2020.
813 Highwood, E. J., and Hoskins, B. J.: The tropical tropopause, Q. J. R. Meteorol. Soc.,
814 124(549), 1579-1604, DOI: 10.1002/qj.49712454911, 1998.
815 Hitchcock, P.: On the value of reanalysis prior to 1979 for dynamical studies of
816 stratosphere-troposphere coupling, Atmos. Chem. Phys., 19, 2749-2764,
817 https://doi.org/10.5194/acp-19-2749-2019, 2019
818 Holton, J. R., Haynes, P. H., McIntyre, M. E., Douglass, A. R., Rood, R. B., and
819 Pfister, L.: Stratosphere-troposphere exchange, Rev. Geophys, 33,
820 403-439, https://doi.org/10.1029/95RG02097, 1995.
821 Hosking, J. S., Russo, M. R., Braesicke, P., and Pyle, J. A.: Tropical convective
822 transport and the Walker circulation, Atmos. Chem. Phys., 12, 9791-9797,
823 doi:10.5194/acp-12-9791-2012, 2012
824 Hu, D., Guan, Z., Tian, W., and Ren, R.: Recent strengthening of the stratospheric
825 Arctic vortex response to warming in the central North Pacific, 9, 1697,
826 https://doi.org/10.1038/s41467-018-04138-3, 2018.
827 Hu, D., Guo, Y., Wang, F., Xu, Q., Li, Y., Sang, W., Wang, X., and Liu, M.:
828 Brewer-Dobson circulation: Recent-Past and near-future trends simulated by
829 chemistry-climate models, Adv. Meteorol., 2017, 1-13,
830 https://doi.org/10.1155/2017/2913895, 2017.
831 Hu, D., Tian, W., Guan, Z., Guo, Y., and Dhomse, S.: Longitudinal asymmetric trends
832 of tropical cold-point tropopause temperature and their link to strengthened
833 Walker circulation, J. Climate, 29(21), 7755–7771,
834 https://doi.org/10.1175/JCLI-D-15-0851.1, 2016.
835 Hu, P., Huangfu, J., Chen, W., and Huang, R.: Impacts of early/late South China Sea
836 summer monsoon withdrawal on tropical cyclone genesis over the western North
837 Pacific, Clim. Dynam., 55(19), 1507-1520,
838 https://doi.org/10.1007/s00382-020-05339-7, 2020.
839 Huang, L., Jiang, J. H., Murray, L. T., Damon, M. R., Su, H., and Livesey, N.:
840 Evaluation of UTLS carbon monoxide simulations in GMI and GEOS-Chem
841 chemical transport models using Aura MLS observations, Atmos. Chem. Phys.,

16, 5641-5663, doi:10.5194/acp-16-5641-2016, 2016.

Kobayashi, S., Ota, Y., Harada, Y., Ebita, A., Moriya, M., and Onoda, H., et al.: The JRA-55 Reanalysis: General specifications and basic characteristics, J. Meteorol. Soc. Jpn., 93, 5-48, DOI:10.2151/jmsj.2015-001, 2015.

Krüger, K., Tegtmeier, S., and Rex, M.: Long-term climatology of air mass transport through the Tropical Tropopause Layer (TTL) during NH winter, Atmos. Chem. Phys., 8, 813–823, doi:10.5194/acpd-7-13989-2007, 2008.

L'Heureux, M. L., Lee, S., and Lyon, B.: Recent multidecadal strengthening of the Walker circulation across the tropical Pacific, Nat. Clim. Change, 3, 571–576, doi: 10.1038/nclimate1840, 2013.

Levine, J. G., Braesicke, P., Harris, N. R. P., Pyle, J. A.: Seasonal and inter-annual variations in troposphere-to-stratosphere transport from the tropical tropopause layer, Atmos. Chem. Phys., 8, 3689-3703, DOI:10.5194/acpd-8-489-2008, 2008.

Levine, J. G., Braesicke, P., Harris, N. R. P., Savage, N. H., and Pyle, J. A.: Pathways and timescales for troposphere-to-stratosphere transport via the tropical tropopause layer and their relevance for very short lived substances, J. Geophys. Res., 112, D04308, doi:10.1029/2005JD006940, 2007.

Liebmann, B., and Smith, C. A.: Description of a complete (interpolated) outgoing longwave radiation dataset, B. Am. Meteorol. Soc., 77, 1275-1277, doi: 10.1175/1520-0477(1996)077<1255:EA>2.0.CO;2, 1996.

Livesey, N. J., Logan, J. A., Santee, M. L., Waters, J. W., Doherty, R. M., Read, W. G., Froidevaux, L., and Jiang, J. H.: Interrelated variatinos of O3, CO and deep convection in the tropical/subtropical upper troposphere observed by the Aura Microwave Lim Sounder (MLS) during 2004-2011, Atmos. Chem. Phys, 13, 579-598, doi:10.5194/acp-13-579-2013, 2013.

Livesey, N. J., Read,W. G.,Wagner, P. A., Froidevaux, L., Lambert, A., Manney, G. L., Millán, L., Pumphrey, H. C., Santee, M. L., Schwartz, M. J., Wang, S., Fuller, R. A., Jarnot, R. F., Knosp, B. W., and Martinez, E.: EOS MLS Version 4.2x Level 2 data quality and description document, Jet Propulsion Laboratory, California Institute of Technology, Pasadena, CA, 2015.

872 Lin, P., Ming, Y., and Ramaswamy, V.: Tropical climate change control of the lower
873 stratospheric circulation, Geophys. Res. Lett., 42(3), 941-948, doi:
874 10.1002/2014GL062823, 2015.
875 Logan, J. A., Megretskaia, I. A., Nassar, R., Murray, L. T., Zhang, L., Bowman, K. W.,
876 Worden, H. M., and Luo, M.: Effects of the 2006 El Niño on tropospheric
877 composition as revealed by data from the Tropospheric Emission Spectrometer
878 (TES), Geophys. Res. Lett., 35, L03816,
879 https://doi.org/10.1029/2007GL031698, 2008.
880 Long, C. S., Fujiwara, M., Davis, S., Mitchell, D. M., and Wright, C. J.: Climatology
881 and interannual variability of dynamic variables in multiply reanalyses evaluated
882 by the SPARC Reanalysis Intercomparison Project (S-RIP), Atmos. Chem. Phys.,
883 17, 14593-14629, https://doi.org/10.5194/acp-17-14593-2017, 2017.
884 Lu, J., Vecchi, G. A., and Reichler, T.: Expansion of the Hadley cell under global
885 warming, Geophys. Res. Lett., 34(6), L06805, doi:10.1029/2006GL028443,
886 2007
887 Lu, J., Xie, F., Sun, C., Luo, J., Cai, Q., Zhang, J., Li, J., and Tian, H.: Analysis of
888 factors influencing tropical lower stratospheric water vapor during 1980–2017,
889 npj Clim. Atmos. Sci., 3(1), 35, https://doi.org/10.1038/s41612-020-00138-7,
890 2020.
891 Ma, S., and Zhou, T.: Robust Strengthening and Westward Shift of the Tropical
892 Pacific Walker Circulation during 1979–2012: A Comparison of 7 Sets of
893 Reanalysis Data and 26 CMIP5 Models, J. Climate, 29, 3097–3118, doi:
894 10.1175/JCLI-D-15-0398.1, 2016.
895 Marsh, D. R., Mills, M. J., Kinnison, D. E., Lamarque, J., Calvo, N., and Polvani, L.
896 M.: Climate change from 1850 to 2005 simulated in CESM1 (WACCM), J.
897 Climate, 26, 7372-7391, https://doi.org/10.1175/JCLI-D-12-00558.1, 2013.
898 McGregor, S., Timmermann, A., Stuecker, M. F., England, M. H., Merrifield, M., Jin,
899 F., and Chikamoto, Y.: Recent Walker circulation strengthening and Pacifific
900 cooling amplifified by Atlantic warming, Nat. Clim. Change, 4, 888–882,
901 https://doi.org/10.1038/nclimate2330, 2014.

902 Meng, Q., Latif, M., Park, W., Keenlyside, N. S., Semenov, V. A., and Martin, T.:
903 Twentieth century Walker circulation change: Data analysis and model
904 experiments, Clim. Dynam., 38, 1757–1773,
905 https://doi.org/10.1007/s00382-011-1047-8, 2012.
906 Minganti, D., Chabrillat, S., Christophe, Y., Errera, Q., Abalos, M., Prignon, M.,
907 Kinnison, D. E., and Mahieu, E.: Climatological impact of the Brewer–Dobson
908 circulation on the N2O budget in WACCM, a chemical reanalysis and a CTM
909 driven by four dynamical reanalyses, Atmos. Chem. Phys., 20, 12609–12631,
910 https://doi.org/10.5194/acp-20-12609-2020, 2020.
911 Navarro, M. A., Atlas, E. L., Saiz-Lopez, A., Rodriguez-Lloveras, X., Kinnison, D. E.,
912 Lamarque, J., Tilmes, S., Filus, M., and Harris, N. R. P., et al.: Airborne
913 measurements of organic bromine compounds in the Pacific tropical tropopause
914 layer, P. Natl. Acad. Sci. USA, 112, 13789-13793, doi:10.1073/pnas.1511463112,
915 2015.
916 Newell, R. E., and Gould-Stewart, S.: A stratospheric fountain? J. Atmos. Sci., 38,
917 2789–2796, DOI: 10.1175/1520-0469(1981)038<2789:ASF>2.0.CO;2, 1981.
918 Newton, R., Vaughan, G., Hintsa, E., Filus, M. T., Pan, L. L., and Honomichl, S., et al.:
919 Observations of ozone-poor air in the tropical tropopause layer, Atmos. Chem.
920 Phys., 18, 5157–5171, https://doi.org/10.5194/acp-18-5157-2018, 2018.
921 Pan, L. L., Atlas, E. L., Salawitch, R. J., Honomichl, S. B., Bresch, J. F., and Randel,
922 W. J., et al.: The Convective Transport of Active Species in the Tropics
923 (CONTRAST) Experiment, B. Am. Meteorol. Soc., 98(1), 106-128,
924 DOI: 10.1175/BAMS-D-14-00272.1, 2016.
925 Pan, L. L., Honomichl, S. B., Thornberry, T., Rollins, A., Bui, T. P., Pfister, L., and
926 Jensen E. E.: Observational Evidence of Horizontal Transport-Driven
927 Dehydration in the TTL, Geophys. Res. Lett., 46(13), 7848-7856,
928 DOI: 10.1029/2019GL083647, 2019.
929 Qie, K., Qie, X., and Tian, W.: Increasing trend of lightning activity in the South Asia
930 region, Sci. Bull., 66, 78-84, https://doi.org/10.1016/j.scib.2020.08.033, 2021.
931 Randel, W. J., and Jensen, E. J.: Physical processes in the tropical tropopause layer

and their roles in a changing climate, Nat. Geosci., 6, 169–176, DOI:10.1038/ngeo1733, 2013.

Randel, W. J., Park, M., Emmons, L., Kinnison, D., Bernath, P., Walker, K. A., Boone, C., and Pumphrey. H., Asian monsoon transport of pollution to the Stratosphere, Science, 328, 611-613, DOI: 10.1126/science.1182274, 2010.

Rao, J., Yu, Y., Guo, D., Shi, C., Chen, D., and Hu, D.: Evaluating the Brewer-Dobson circulation and its responses to ENSO, QBO, and the solar cycle in different reanalyses, Earth Planet. Phys., 3(2), 1-16, http://doi.org/10.26464/epp2019012, 2019.

Rayner, N., Parker, D., Horton, E., Folland, C. K., Alexander, L., and Rowell, D. P., et al.: Global analyses of sea surface temperature, sea ice, and night marine air temperature since the late nineteenth century, J. Geophys. Res., 108(D14), 4407, doi:10.1029/2002JD002670, 2003.

Rosenlof, K. H. How water enters the stratosphere, Science, 302, 1691-1692, doi:10.1126/science.1092703, 2003.

Ryu, J., and Lee, S.: Effect of tropical waves on the tropical tropopause transition layer upwelling, J. Atmos. Sci., 67(10), 3130-3148, DOI: 10.1175/2010JAS3434.1, 2010.

Saiz-Lopez, A., and von Glasow, R.: Reactive halogen chemistry in the troposphere, Chem. Soc. Rev., 41, 6448–6472, DOI:10.1039/c2cs35208g, 2012.

Schoeberl, M. R., Jensen, E. J., Pfister, L., Ueyama, R., Avery, M., and Dessler, A. E.: Convective hydration of the upper troposphere and lower stratosphere, J. Geophys. Res., 123(9), 4583-4593, https://doi.org/10.1029/2018JD028286, 2018.

Sherwood, S. C.: A stratospheric “drain” over the maritime continent, Geophys. Res. Lett., 27(5), 677-680, https://doi.org/10.1029/1999GL010868, 2000.

Shindell, D. T., Pechony, O., Voulgarakis, A., Faluvegi, G., Nazarenko, L., Lamarque, J.-F., Bowman, K., Milly, G., Kovari, B., Ruedy, R., and Schmidt, G. A.: Interactive ozone and methane chemistry in GISS-E2 historical future climate simulations, Atmos. Chem. Phys., 13, 2653-2689, doi:10.5194/acp-13-2653-2013, 2013.

962 Shirley, D., Stanley, W., & Daniel, C.: Statistics for Research (Third Edition), (p. 627),
963 Hoboken, New Jersey: John Wiley & Sons Inc., 2004.
964 Simmons, A. J., Poli, P., Dee, D. P., Berrisford, P., Hersbach, H., Kobayashi, S., and
965 Peubey, C.: Estimating lowfrequency variability and trends in atmospheric
966 temperature using ERA-Interim, Q. J. Roy. Meteorol. Soc., 140, 329 – 353,
967 https://doi.org/10.1002/qj.2317, 2014.
968 Sinnhuber, B.-M., Sheode, N., Sinnhuber, M., Chipperfield, M. P., and Feng, W.: The
969 contribution of anthropogenic bromine emis sions to past stratospheric ozone
970 trends: a modelling study, Atmos. Chem. Phys., 9, 2863 – 2871,
971 doi:10.5194/acp-9-2863-2009, 2009.
972 Solomon, S., Rosenlof, K. H., Portmann, R. W., Daniel, J. S., Davis, S. M., Sanford, T.
973 J., and Plattner, G.-K.: Contributions of stratospheric water vapor to decadal
974 changes in the rate of global warming, Science, 327, 1219-1223,
975 DOI:10.1126/science.1182488, 2010.
976 Tegtmeier, S., Anstey, J., Davis, S., Dragani, R., Harada, Y., Ivanciu, I., Kedzierski, R.
977 P., Krüger, K., Legras, B., Long, C., Wang, J. S., Wargan, K., and Wright, J. S.:
978 Temperature and tropopause characteristics from reanalyses data in the tropical
979 tropopause layer, Atmos. Chem. Phys., 20, 753-770,
980 https://doi.org/10.5194/acp-20-753-2020, 2020.
981 Tokinaga, H., Xie, S. P., Deser, C., Kosaka, Y., and Okumura, Y. M.: Slowdown of the
982 Walker circulation driven by tropical Indo-Pacifific warming. Nature, 491,
983 439–443, DOI: 10.1038/nature11576, 2012.
984 Uma, K. N., Das, S. S., Ratnam, M. V., and Suneeth, K. V.: Assessment of vertical air
985 motion among reanalyses and qualitative comparison with very-high-frequency
986 radar measurements over two tropical stations, Atmos. Chem. Phys., 21,
987 2083-2103, https://doi.org/10.5194/acp-21-2083-2021, 2021.
988 Wales, P. A., Salawitch, R. J., Nicely, J. M., Anderson, D. C., Canty, T. P. and Baidar,
989 S., et al.: Stratospheric injection of Brominated very short-lived substances:
990 Aircraft observations in the western Pacific and representation in global models,
991 J. Geophys. Res., 123(10), 5690-5719, https://doi.org/10.1029/2017JD027978,

2017.

Wang, S., Schmidt, J. A., Baidar, S., Coburn, S., Dix, B., and Koenig, T. K., et al.: Active and wide-spread halogen chemistry in the tropical and subtropical free troposphere, P. Natl. Acad. Sci. USA, 112, 9281–9286, DOI: 10.1073/pnas.1505142112, 2015.

Wang, W., Matthes, K., and Schmidt, T.: Quantifying contributions to the recent temperature variability in the tropical tropopause layer, Atmos. Chem. Phys., 15, 5815–5826, doi:10.5194/acp-15-5815-2015, 2015.

Wang, W., Matthes, K., Omarani, N.-E., and Latif, M.: Decadal variability of tropical tropopause temperature and its relationship to the Pacific Decadal Oscillation, Sci. Rep., 6, 29537, https://doi.org/10.1038/srep29537, 2016.

Wang, W., Tian, W., Dhomse, S., Xie, F., Shu, J., and Austin, J.: Stratospheric ozone depletion from future nitrous oxide increases, Atmos. Chem. Phys., 14, 12967-12982, doi:10.5194/acp-14-12967-2014, 2014.

Webster, P. J., Lukas, R.: TOGA COARE: the coupled ocean-atmosphere response experiment, B. Am. Meteorol. Soc., 73(9), 1377-1416, DOI: 10.1175/1520-0477(1992)073<1377:TCTCOR>2.0.CO;2, 1992.

Webster, P. J., Clayson, C. A., Curry, J. A.: Clouds, radiation, and the diurnal cycle of sea surface temperature in the tropical western Pacific, J. Climate, 8(8), 1712-1730, DOI: 10.1175/1520-0442(1996)009<1712:CRATDC>2.0.CO;2, 1996.

WMO.: Low-cost Sensors for the Measurement of Atmospheric Composition: Overview of Topic and Future Applications, 2018.

Xie, F., Li, J., Tian, W., Feng, J., and Huo, Y.: Signals of El Niño Modoki in the tropical tropopause layer and stratosphere, Atmos. Chem. Phys., 12, 5259-5273, doi:10.5194/acp-12-5259-2012, 2012.

Xie, F., Li, J., Tian, W., Li, Y., and Feng, J.: Indo-Pacific Warm Pool Area Expansion, Modoki Activity, and Tropical Cold-Point Tropopause Temperature Variations, Sci. Rep., 4, 4552, https://doi.org/10.1038/srep04552, 2014a.

Xie, F., Li, J., Tian, W., Zhang, J., and Shu, J.: The impacts of two types of El Niño on

global ozone variations in the last three decades, Adv. Atmos. Sci., 31(5), 1113-1126, doi: 10.1007/s00376-013-3166-0, 2014b.

Xie, F., Tian, W., Zhou, X., Zhang, J., Xia, Y., and Lu, J.: Increase in lower stratospheric water vapor in the past 100 years related to tropical Atlantic warming, *Geophys. Res. Lett.*, 47, e2020GL090539, DOI: 10.1029/2020GL090539, 2020.

Zhou, X., Chen, Q., Li, Y., Zhao, Y., Lin, Y., and Jiang, Y.: Impacts of the Indo-Pacific warm pool on lower stratospheric water vapor: Seasonality and hemispheric contrasts, J. Geophys. Res., 126, e2020JD034363, DOI: 10.1029/2020JD034363, 2021.

Figure captions:

Fig. 1. The climatological mean (averaged over 1958-2017) values of 150 hPa w (10^{-2} m s^{-1}) in different months derived from the JRA55 data.

Fig. 2. Trends of vertical velocity and horizontal winds at 150 hPa, 500 hPa, 700 hPa in NDJFM derived from JRA55, ERA5, and MERRA2 data. The trends of horizontal winds (arrows, units: 10^{-1} m s^{-1} a^{-1}) and vertical velocity (shading, units: 10^{-4} m s^{-1} a^{-1}) at (a) 150 hPa; (d) 500 hPa; and (g) 700 hPa from JRA55 in NDJFM during 1958-2017. (b), (e), and (h) are the same as (a), (d), and (g) but for the results from ERA5. (c), (f) and (i) are the same as (a), (d), and (g) except that the trends are during 1980-2017 and the wind field data are from MERRA2. The vertical velocity trends over the dotted regions are statistically significant at the 95% confidence level. The white areas denote missing values. The black rectangles denote the TWP region (20°S-10°N, 100°E-180°E).

Fig. 3. The time series of the standardized intensity of the upward motion over the tropical western Pacific (20°S-10°N, 100°E-180°E) at (a) 150 hPa; (b) 500 hPa; and

(c) 700 hPa extracted from JRA55 (red), ERA5 (black) and MERRA2 (blue) datasets. The straight lines in each figure indicate the linear trends. The solid lines denote the linear trends are significant at the 95% confidence level, while the dashed lines denote the linear trends are significant at the 90% confidence level.

Fig. 4. Trends of (a) observed outgoing longwave radiation (OLR, units: W m^{-2} a^{-1}) provided by NOAA during 1974-2017; (b) cold-point tropopause temperature (CPTT, units: 10^{-1} K a^{-1}) derived from JRA55 data and (c) SST (K a^{-1}) derived from HadISST during 1958-2017 in NDJFM. (d) The correlation coefficients between the intensity of the upward motion at 150 hPa over the TWP and SST in NDJFM during 1958-2017 with the linear trends removed. The trends and correlation coefficients over the dotted regions are statistically significant at the 95% confidence level. The black rectangles denote the TWP region (20°S-10°N, 100°E-180°E).

Fig. 5. The trends of vertical velocity and horizontal winds at 150 hPa, 500 hPa, and 700 hPa in NDJFM during 1958-2017 in the Control and Fixsst simulations as well as their difference. The trends of 150 hPa *w* (shading, units: 10^{-4} m s^{-1} a^{-1}) and horizontal winds (arrows; 10^{-1} m s^{-1} a^{-1}) from (a) Control simulation; (b) Fixsst simulation; and (c) difference between the Control simulation and the Fixsst simulation in NDJFM during 1958-2017. (d)-(f) are similar to (a)-(c) but for the results at 500 hPa. (g)-(i) are similar to (d)-(f) but for the results at 700 hPa. The vertical velocity trends over the dotted regions are statistically significant at the 95% confidence level. The black rectangles denote the TWP region (20°S-10°N, 100°E-180°E).

Fig. 6. The difference of vertical velocity (shading, units: 10^{-2} m s^{-1}) and horizontal

winds (arrows, units: m s^{-1}) at (a) 150 hPa; (b) 500 hPa; and (c) 700 hPa in NDJFM between experiments R1 and R2. The differences between vertical velocity over the dotted regions are statistically significant at the 95% confidence level. The black rectangles denote the TWP region (20°S-10°N, 100°E-180°E).

Fig. 7. Trends of OLR (W m^{-2} a^{-1}) (a)-(c), CPTT (shading, units: 10^{-1} K a^{-1}) and 100 hPa streamfunction (contour, units: 10^{6} m^{2} s^{-1} a^{-1}) (d)-(f), and 70 hPa water vapor concentration (units: 10^{-2} ppmv a^{-1}) (g)-(i) in NDJFM during 1958-2017 in the Control and Fixsst simulations as well as their difference. (a), (d), and (g) are the results in the Control simulation; (b), (e), and (h) are the results in the Fixsst simulation; (c), (f), and (i) are the results of the difference between the Control and Fixsst simulations. The trends in (a)-(c) and (g)-(i) over the dotted regions are statistically significant at the 95% confidence level. The CPTT trends in (d)-(f) over the dotted regions are statistically significant at the 95% confidence level. The black rectangles denote the TWP region (20°S-10°N, 100°E-180°E).

Fig. 8. The trends of CO derived from the MOPITT and MLS data. (a) The trends of CO (10^{-1} ppbv a^{-1}) at 215 hPa using MLS data in NDJFM during 2005-2017. (b) The trends of CO (10^{-1} ppbv a^{-1}) at 200 hPa using MOPITT data in NDJFM during 2000-2017. The trends of CO over the dotted region are statistically significant at the 90% confidence level.

Fig. 9. The trends of 150 hPa CO concentration (10^{-4} ppmv a^{-1}) from (a) Control simulation; (b) Fixsst simulation; and (c) difference between the Control simulation and the Fixsst simulation in NDJFM during 1958-2017. The trends in (a)-(c) over the

dotted regions are statistically significant at the 95% confidence level. The black rectangles denote the TWP region (20°S-10°N, 100°E-180°E).

Fig. 10. Latitude-pressure cross sections of the trends of (a)-(c) zonal mean CO concentration (10^{-4} ppmv a^{-1}) and (d)-(f) CO concentration (10^{-4} ppmv a^{-1}) over the TWP (100°E-180°E) in NDJFM during 1958-2017 in the Control simulation and Fixsst simulation as well as their difference. (a) and (d) are the CO trends in the Control simulation. (b) and (e) are the results in the Fixsst simulation. (c) and (f) are the results derived from the difference between the Control and Fixsst simulations. The trends over the dotted regions are statistically significant at the 95% confidence level.

Fig. 11. Latitude-pressure cross sections of the trends of (a)-(c) the zonal mean w (10^{-4} m s^{-1} a^{-1}) and v (10^{-1} m s^{-1} a^{-1}) and (d)-(f) w (10^{-4} m s^{-1} a^{-1}) and v (10^{-1} m s^{-1} a^{-1}) over the TWP (100°E-180°E) in NDJFM during 1958-2017 in the Control simulation and Fixsst simulation as well as their difference. (a) and (d) are the trends of w and v in the Control simulation. (b) and (e) are the results in the Fixsst simulation. (c) and (f) are the results derived from the difference between the Control and Fixsst simulations. The shadings denote the trends of the w (10^{-4} m s^{-1} a^{-1}). The trends over the dotted regions are statistically significant at the 90% confidence level.

Fig. 12. Trends of the BDC (vectors, units in the horizontal and vertical components are 10^{-2} and 10^{-5} m s^{-1} a^{-1}, respectively) calculated using the TEM formula from (a) JRA55; (b) Control simulation; (c) Fixsst simulation; and (d) difference between the Control simulation and the Fixsst simulation in NDJFM during 1958-2017. The

1114 shadings are the trends of the w^* (10^{-5} m s^{-1} a^{-1}). The trends of the vertical velocity

1115 over the dotted regions are statistically significant at the 90% confidence level.

1116

Figures

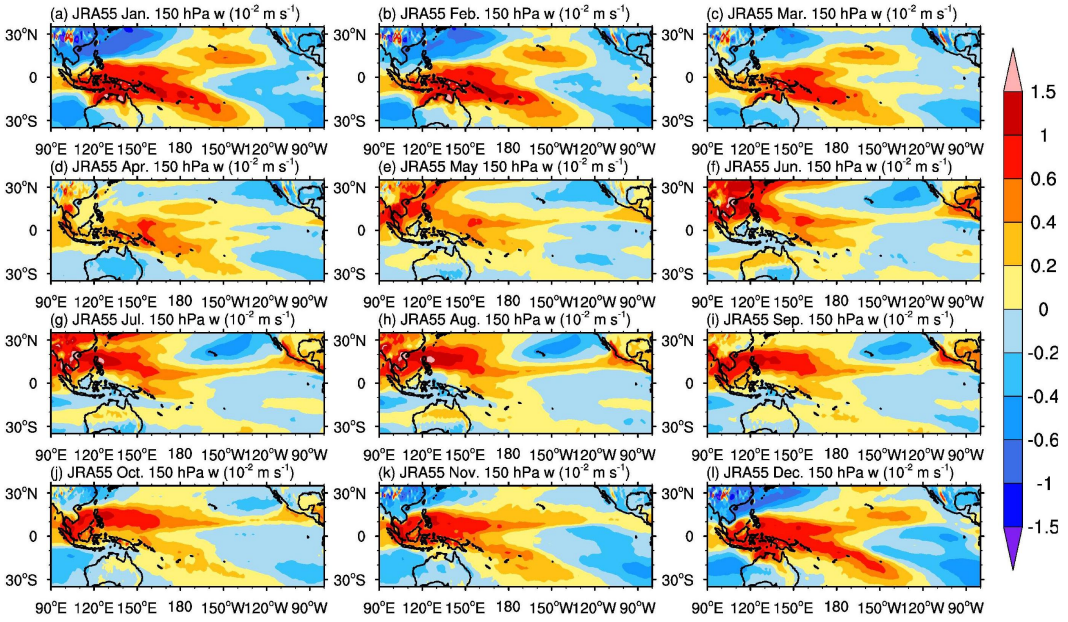

Fig. 1. The climatological mean (averaged over 1958-2017) values of 150 hPa *w* (10^{-2} m s^{-1}) in different months derived from the JRA55 reanalysis data.

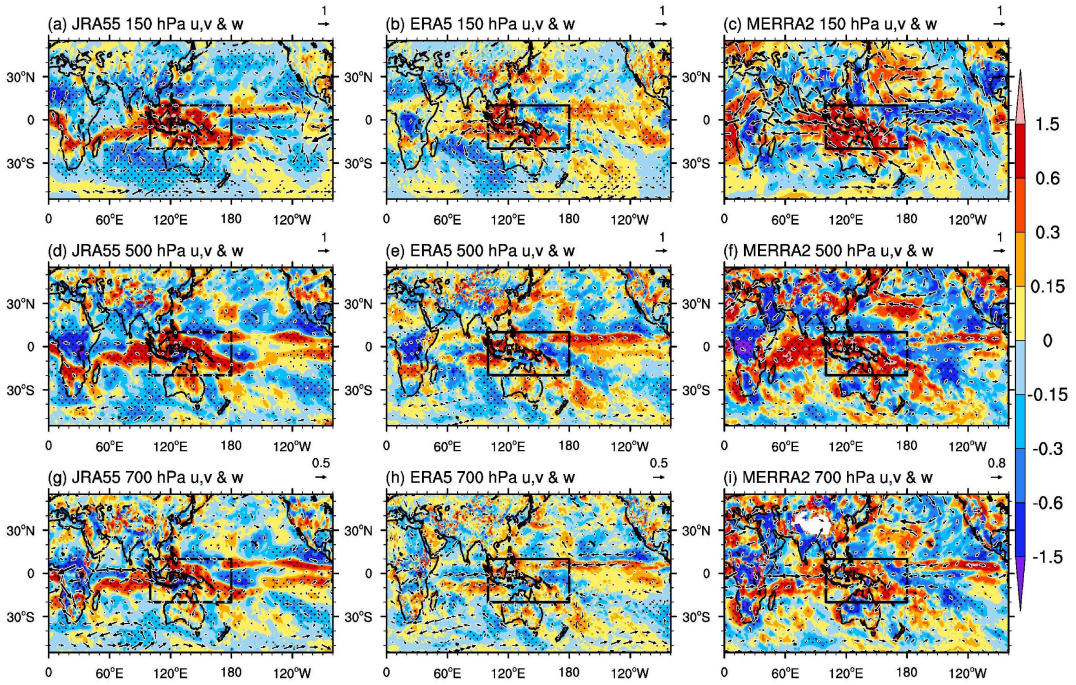

Fig. 2. Trends of vertical velocity and horizontal winds at 150 hPa, 500 hPa, 700 hPa in NDJFM derived from JRA55, ERA5, and MERRA2 data. The trends of horizontal winds (arrows, units: 10^{-1} m s^{-1} a^{-1}) and vertical velocity (shading, units: 10^{-4} m s^{-1} a^{-1}) at (a) 150 hPa; (d) 500 hPa; and (g) 700 hPa from JRA55 in NDJFM during 1958-2017. (b), (e), and (h) are the same as (a), (d), and (g) but for the results from ERA5. (c), (f) and (i) are the same as (a), (d), and (g) except that the trends are during 1980-2017 and the wind field data are from MERRA2. The vertical velocity trends over the dotted regions are statistically significant at the 95% confidence level. The white areas denote missing values. The black rectangles denote the TWP region (20°S-10°N, 100°E-180°E).

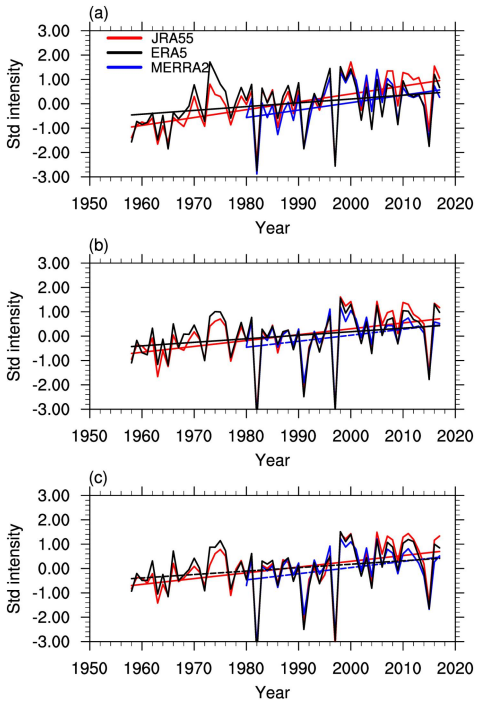

Fig. 3. The time series of the standardized intensity of the upward motion over the tropical western Pacific (20°S-10°N, 100°E-180°E) at (a) 150 hPa; (b) 500 hPa; and (c) 700 hPa extracted from JRA55 (red), ERA5 (black) and MERRA2 (blue) datasets. The straight lines in each figure indicate the linear trends. The solid lines denote the linear trends are significant at the 95% confidence level, while the dashed lines denote the linear trends are significant at the 90% confidence level.

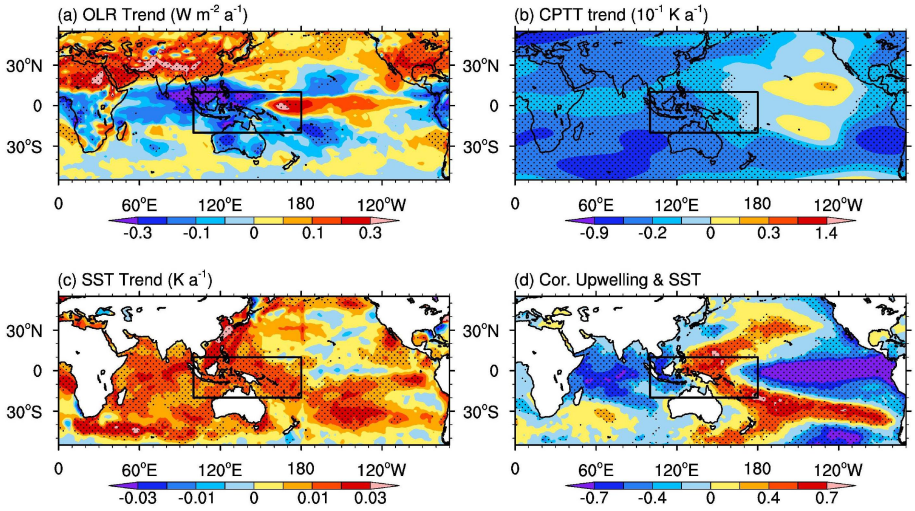

1143

1144 **Fig. 4.** Trends of (a) observed outgoing longwave radiation (OLR, units: W m^{-2} a^{-1})
1145 provided by NOAA during 1974-2017; (b) cold-point tropopause temperature (CPTT,
1146 units: 10^{-1} K a^{-1}) derived from JRA55 data and (c) SST (K a^{-1}) derived from HadISST
1147 during 1958-2017 in NDJFM. (d) The correlation coefficients between the intensity of
1148 the upward motion at 150 hPa over the TWP and SST in NDJFM during 1958-2017
1149 with the linear trends removed. The trends and correlation coefficients over the dotted
1150 regions are statistically significant at the 95% confidence level. The black rectangles
1151 denote the TWP region (20°S-10°N, 100°E-180°E).

1152

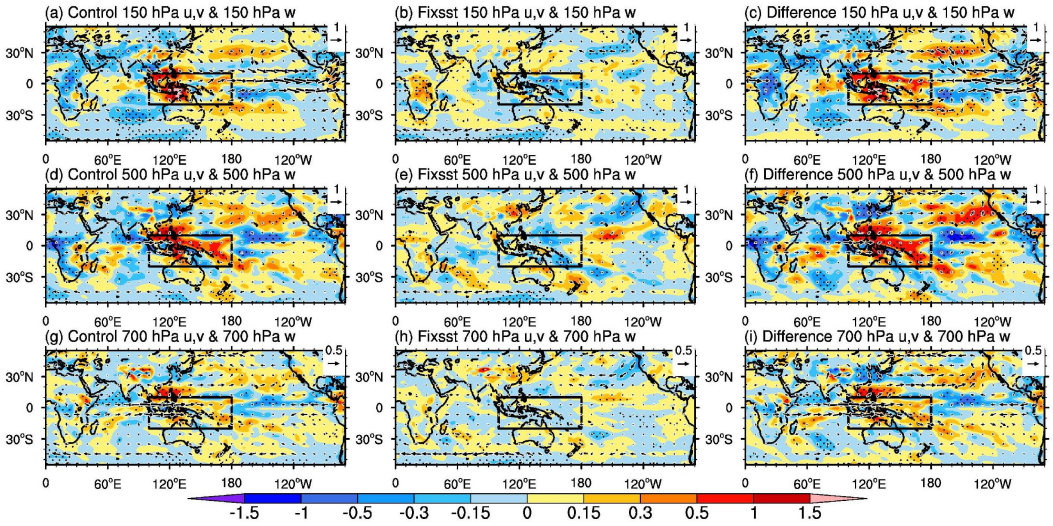

1153

1154 **Fig. 5.** The trends of vertical velocity and horizontal winds at 150 hPa, 500 hPa, and

1155 700 hPa in NDJFM during 1958-2017 in the Control and Fixsst simulations as well as

1156 their difference. The trends of 150 hPa *w* (shading, units: 10^{-4} m s^{-1} a^{-1}) and horizontal

1157 winds (arrows; 10^{-1} m s^{-1} a^{-1}) from (a) Control simulation; (b) Fixsst simulation; and

1158 (c) difference between the Control simulation and the Fixsst simulation in NDJFM

1159 during 1958-2017. (d)-(f) are similar to (a)-(c) but for the results at 500 hPa. (g)-(i)

1160 are similar to (d)-(f) but for the results at 700 hPa. The vertical velocity trends over

1161 the dotted regions are statistically significant at the 95% confidence level. The black

1162 rectangles denote the TWP region (20°S-10°N, 100°E-180°E).

1163

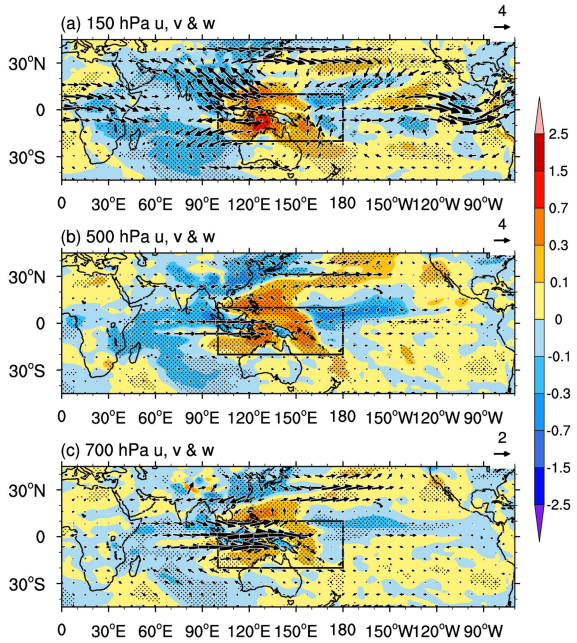

Fig. 6. The difference of vertical velocity (shading, units: 10^{-2} m s^{-1}) and horizontal winds (arrows, units: m s^{-1}) at (a) 150 hPa; (b) 500 hPa; and (c) 700 hPa in NDJFM between experiments R1 and R2. The differences between vertical velocity over the dotted regions are statistically significant at the 95% confidence level. The black rectangles denote the TWP region (20°S-10°N, 100°E-180°E).

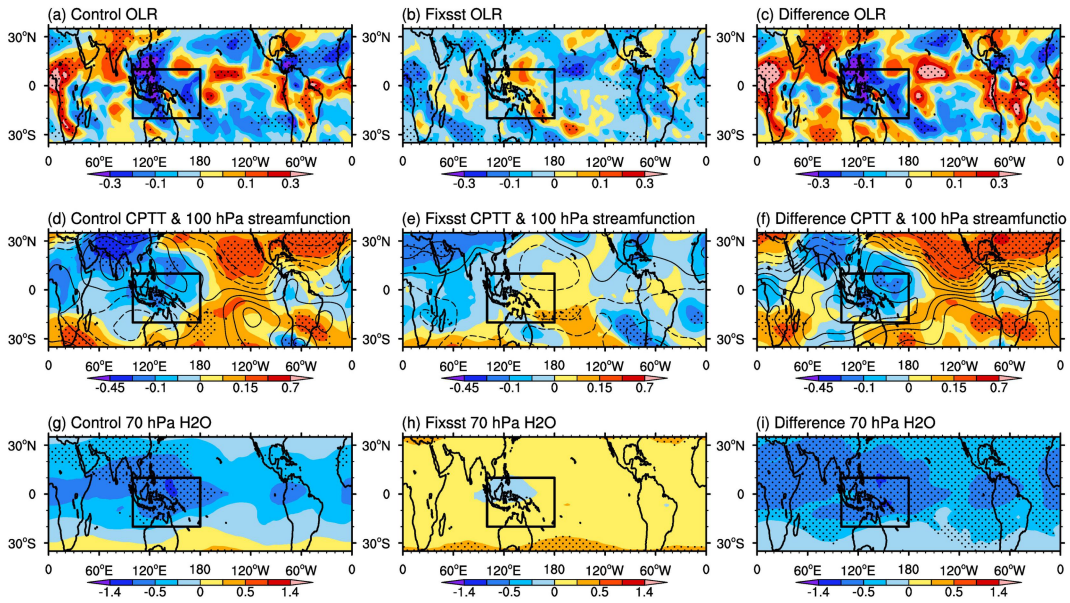

1172

1173 **Fig. 7.** Trends of OLR (W m^{-2} a^{-1}) (a)-(c), CPTT (shading, units: 10^{-1} K a^{-1}) and 100

1174 hPa streamfunction (contour, units: 10^{6} m^{2} s^{-1} a^{-1}) (d)-(f), and 70 hPa water vapor

1175 concentration (units: 10^{-2} ppmv a^{-1}) (g)-(i) in NDJFM during 1958-2017 in the

1176 Control and Fixsst simulations as well as their difference. (a), (d), and (g) are the

1177 results in the Control simulation; (b), (e), and (h) are the results in the Fixsst

1178 simulation; (c), (f), and (i) are the results of the difference between the Control and

1179 Fixsst simulations. The trends in (a)-(c) and (g)-(i) over the dotted regions are

1180 statistically significant at the 95% confidence level. The CPTT trends in (d)-(f) over

1181 the dotted regions are statistically significant at the 95% confidence level. The black

1182 rectangles denote the TWP region (20°S-10°N, 100°E-180°E).

1183

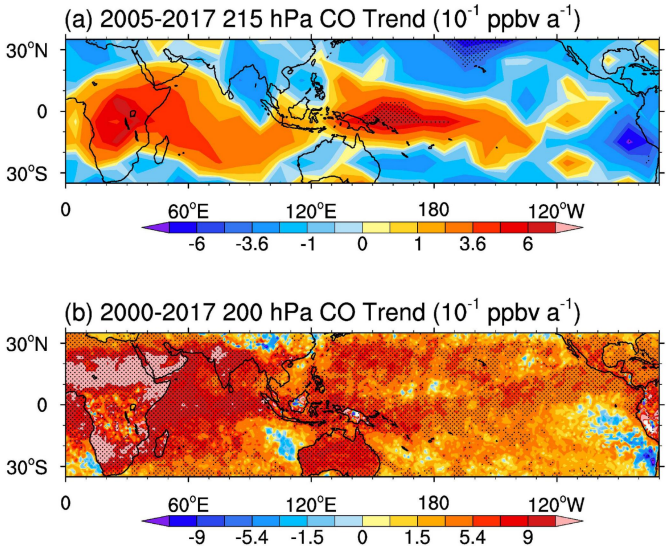

1184

1185 **Fig. 8.** The trends of CO derived from the MOPITT and MLS data. (a) The trends of

1186 CO (10^{-1} ppbv a^{-1}) at 215 hPa using MLS data in NDJFM during 2005-2017. (b) The

1187 trends of CO (10^{-1} ppbv a^{-1}) at 200 hPa using MOPITT data in NDJFM during

1188 2000-2017. The trends of CO over the dotted region are statistically significant at the

1189 90% confidence level.

1190

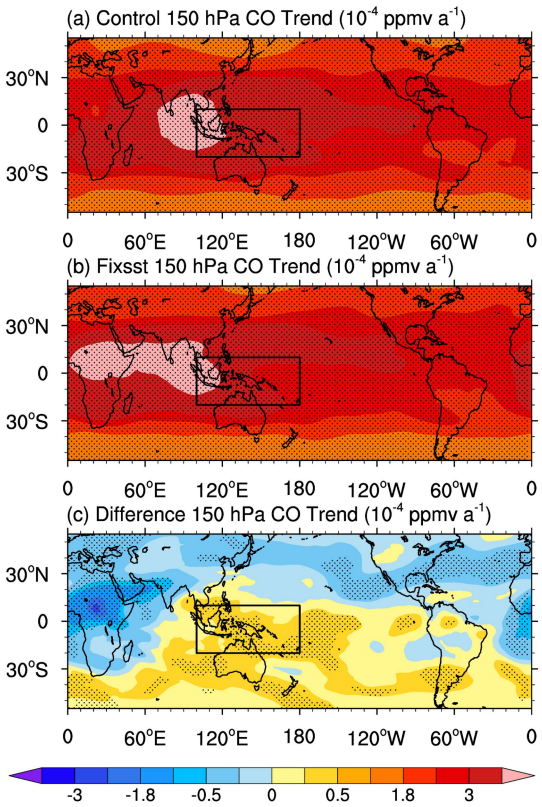

Fig. 9. The trends of 150 hPa CO concentration (10^{-4} ppmv a^{-1}) from (a) Control simulation; (b) Fixsst simulation; and (c) difference between the Control simulation and the Fixsst simulation in NDJFM during 1958-2017. The trends in (a)-(c) over the dotted regions are statistically significant at the 95% confidence level. The black rectangles denote the TWP region (20°S-10°N, 100°E-180°E).

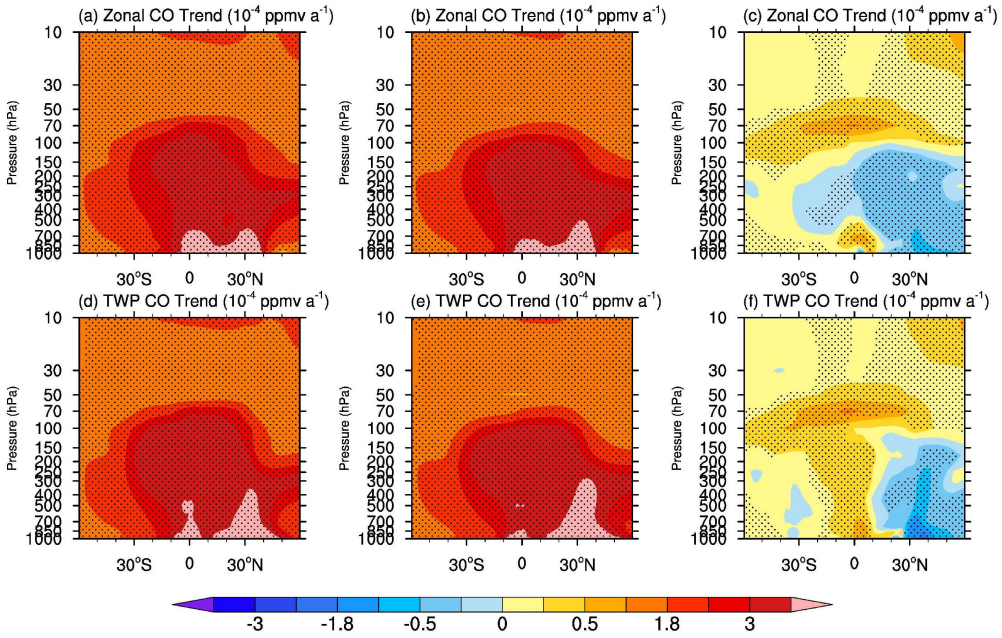

Fig. 10. Latitude-pressure cross sections of the trends of (a)-(c) zonal mean CO concentration (10^{-4} ppmv a^{-1}) and (d)-(f) CO concentration (10^{-4} ppmv a^{-1}) over the TWP (100°E-180°E) in NDJFM during 1958-2017 in the Control simulation and Fixsst simulation as well as their difference. (a) and (d) are the CO trends in the Control simulation. (b) and (e) are the results in the Fixsst simulation. (c) and (f) are the results derived from the difference between the Control and Fixsst simulations. The trends over the dotted regions are statistically significant at the 95% confidence level.

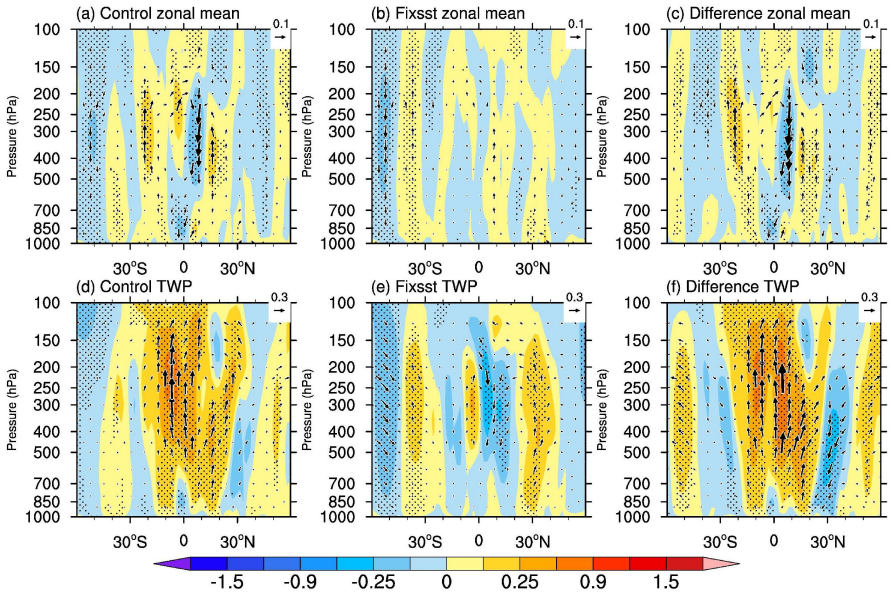

1211

1212 **Fig. 11.** Latitude-pressure cross sections of the trends of (a)-(c) the zonal mean w (10^{-4}

1213 m s^{-1} a^{-1}) and v (10^{-1} m s^{-1} a^{-1}) and (d)-(f) w (10^{-4} m s^{-1} a^{-1}) and v (10^{-1} m s^{-1} a^{-1}) over

1214 the TWP (100°E-180°E) in NDJFM during 1958-2017 in the Control simulation and

1215 Fixsst simulation as well as their difference. (a) and (d) are the trends of w and v in

1216 the Control simulation. (b) and (e) are the results in the Fixsst simulation. (c) and (f)

1217 are the results derived from the difference between the Control and Fixsst simulations.

1218 The shadings denote the trends of the w (10^{-4} m s^{-1} a^{-1}). The trends over the dotted

1219 regions are statistically significant at the 90% confidence level.

1220

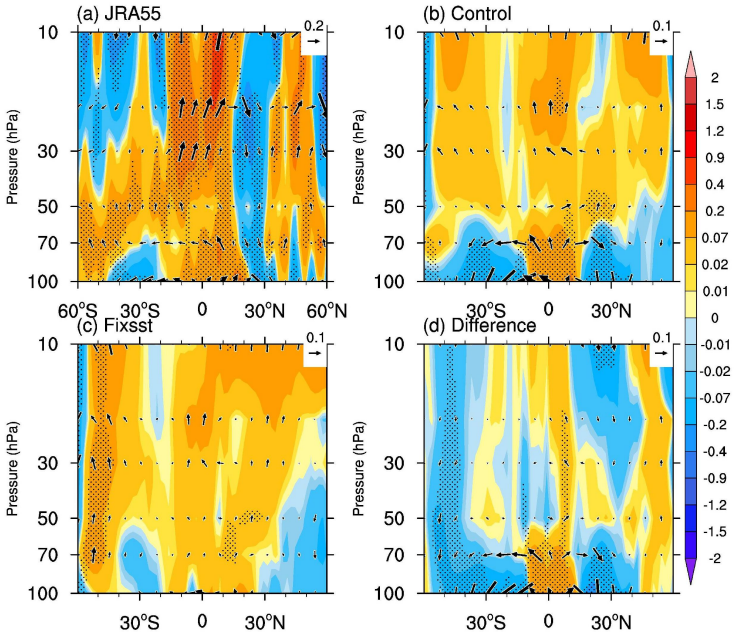

1221

1222 **Fig. 12.** Trends of the BDC (vectors, units in the horizontal and vertical components

1223 are 10^{-2} and 10^{-5} m s^{-1} a^{-1}, respectively) calculated using the TEM formula from (a)

1224 JRA55; (b) Control simulation; (c) Fixsst simulation; and (d) difference between the

1225 Control simulation and the Fixsst simulation in NDJFM during 1958-2017. The

1226 shadings are the trends of the w^* (10^{-5} m s^{-1} a^{-1}). The trends of the vertical velocity

1227 over the dotted regions are statistically significant at the 90% confidence level.

1228